Buchan Prize winner

We are delighted to hear that Adrian Simmons has been awarded the Royal Meteorological Society's Buchan Prize for Meteorology. The Buchan Prize, which commemorates the eminent Scottish meteorologist and climatologist, is awarded annually for a paper (or papers) published in the preceding five years in the Quarterly Journal, the International Journal of Climatology, or Atmospheric Science Letters that is judged to contain the most important original contributions to meteorology.

Adrian Simmons has won the prize for four papers published in the Quarterly Journal of the Royal Meteorological Society. His work is notable for its mastery of the wide range of science that he covers and for his clarity of thinking, and his papers reflect this. They also reflect the very important part he has played in the development of modern numerical weather prediction through his various rôles at the European Centre for Medium-Range Weather Forecasts. The cited papers illustrate his involvement with the development of operational numerical-model and data-assimilation systems. They also discuss how these, and the improvement in observational systems, have been important in the increased predictive skill that has been produced in recent years. Dr Simmons continues to use advanced operational systems for further understanding important aspects of weather and climate. In particular he has produced insights into the behaviour of cold tropical tropopause temperatures and the dryness of the stratosphere. Many congratulations to Adrian.

References

A.J. Simmons, **A.J.**, **Untch**, **A.**, **Jakob**, **C.**, **Källberg**, **P**. and **Undén**, **P.**, 1999: Stratospheric water vapour and tropical tropopause temperatures in ECMWF analyses and multi-year simulations. *Q.J.R. Meteorol. Soc.*, **125**, 353-386

Rabier, **F.**, **Järvinen**, **H.**, **Klinker**, **E.**, **Mahfouf**, **J-F**. and **Simmons**, **A.J.**, 2000: The ECMWF operational implementation of four-dimensional variational assimilation. I: Experimental results with simplified physics. *Q.J.R. Meteorol. Soc.*, **126**, 1143-1170

Temperton, **C.**, **Hortal**, **M.** and **Simmons**, **A.J.**, 2001: A two-time-level semi-Lagrangian global spectral model. *Q.J.R. Meteorol. Soc.*, **127**, 111-127

Simmons, **A.J.** and **Hollingsworth**, **A.**, 2002: Some aspects of the improvement in skill of numerical weather prediction. *Q.J.R. Meteorol. Soc.*, **128**, 649-677

In this issue

European Centre for Medium-Range Weather Forecasts

Shinfield Park, Reading, Berkshire RG2 9AX, UK

Fax: . . . . . .+44 118 986 9450

Telephone: National 0118 949 9000

International . . . . . .+44 118 949 9000

ECMWF Web site . . . . . .http://www.ecmwf.int

The ECMWF Newsletter is published quarterly and contains articles about new developments and systems at ECMWF. Articles about uses and applications of ECMWF forecasts are also welcome from authors working elsewhere (especially those from Member States and Co-operating States).

The ECMWF Newsletter is not a peer-reviewed publication.

Editor: Peter White

Typesetting and Graphics: Rob Hine

Front Cover

An article on freak-wave forecasting is printed on page 24 (cover picture after Hiroshige).

Editorial

This is the 100th issue of the Newsletter and, for interest, on page 2 we publish one of the main articles in issue no. 1 by Daniel Söderman (who was Head of Operations at the time). The progress by the ECMWF since then is illustrated in the article on page 3 by Frederic Vitart about monthly forecasts, which are in a similar stage of development as medium-range forecasts were in 1980. Although still regarded as experimental, the forecasts show a useful level of skill, particularly at certain times of the year, and wider dissemination is planned later this year. Thomas Jung, Adrian Simmons and Mark Rodwell discuss systematic errors in the ECMWF forecasting system on page 14, and illustrate how these have changed with successive model cycles. They focus on Atlantic blocking, intraseasonal variability in the tropics, clouds and the impact of improved aerosol climatology. Peter Janssen provides an insight into the problem of freak-wave prediction on page 24. Finally I would like to draw your attention to the request by Austin Woods on page 30 for background information that would be useful for inclusion in the History of ECMWF that he is writing.

Peter White

Changes to the Operational Forecasting System

Met-7 CSR was re-introduced on 17 December after a processing change at EUMETSAT had created an interruption. NOAA-15 AMSU-A channel 6 was blacklisted on 18 February due to instrumental drift.

A new version of ECMWF model Cycle 28r1 was implemented on 9 March involving the following, mainly minor, technical modifications.

Data assimilation changes

- New snow analysis using the NESDIS snow-cover product;
- Improved use of GOES BUFR winds;
- Improved clouds in the 4D-Var minimization;
- Re-introduction of ERS-2 scatterometer winds (with adjusted pre-screening and limited coverage)
- Variational quality control corrected for 3D-Var (with impacts on the Boundary Condition project and ERA-40 reruns only).

Numerics changes

- Semi-Lagrangian fix for polar vortex instabilities
- Several code modifications in preparation for the L91 version.

Physics changes

- Convection clean-up
- Optimization of linearized physics and more optimizations of the physics code.

Oceanic waves

- Introduction of subgrid-scale (unresolved) bathymetry effects
- A fix to the EPS wave-model interface (Charnock variable)

The overall impact was very small in terms of forecast performance.

Changes and corrections in the dissemination of weather parameters and forecast probabilities (added wind gusts and corrected snowfall descriptors) were made on 30 March.

François Lalaurette

The 100th issue of the ECMWF Newsletter

This is the 100th issue of the Newsletter, the first being published in February 1980. Although the ECMWF had been in existence for five years, 1980 marked the time when the Centre was fully installed in the present building with a state-of-the-art computer system and a forecasting model that was being routinely run to produce medium-range forecasts on an experimental basis, with a selection of the results being transmitted to Member States for assessment. Telecommunications were still a bit rudimentary to some countries, and the forecasts only became formally 'operational' at the start of the following year. The cover picture shows the first attempts at producing non-standard output in the form of a 'pseudo satellite picture'. The survey article by Daniel Söderman (Head of Operations at the time) indicates that, although the computers today are appreciably more powerful and the model very much more sophisticated, the broad objectives of the Centre remain similar 24 years later, though much expanded in scope and capability.

First published in February 1980 in ECMWF Newsletter No 1

A look at ECMWF operational and computing activities

In a surprisingly short time, ECMWF has built up an efficient and well-balanced computer complex with a CRAY-1 'number cruncher', a CDC CYBER 175 'front-end' and a Regnecentralen RC8000 telecommunications system as main components, all being linked via high-speed channels. Telecommunication links between ECMWF and the meteorological offices of the Member States are currently being set up. The first of the medium-speed links, to the Swedish Meteorological and Hydrological Institute in Norrköping, was fully implemented in December 1979 and operates, according to reports received from Sweden, to the complete satisfaction of the users of both the forecast products and the remote batch services of the Centre. Low-speed links have also been established to Yugoslavia, Turkey, Italy, Spain, France, Greece, and the Netherlands.

In parallel with the design, acquisition and implementation of the Centre's computer system, a complex operational forecasting suite, including a sophisticated global forecasting model, has been designed and set up. Operational forecasting tests started in August 1979 and 10-day forecasts have, since then, been run five days per week. A selection of these forecasts has been disseminated to Member States, where they have generally been received with appreciation. The forecasts have also been evaluated internally by Centre staff in order to identify and eliminate deficiencies and bugs in the operational suite.

It must be stressed at this time that the ECMWF forecasts of today should not be seen as 'the final product'. At present the data cut-off time is very early (around 17.30Z). Studies are currently being undertaken to determine the optimal cut-off time, with a view to including 18Z and possibly even some 00Z data. In addition, many improvements to the various modules of the operational suite are being implemented. Important target dates are 1 August 1980, when operational forecasting seven days per week is to be initiated, and 1 January 1981, when dissemination of a selection of ECMWF products to non-Member States via the GTS could start, in accordance with the decision of Council at its tenth session. As well as working to improve the operational suite itself, staff at the Centre are also themselves introducing refinements to the analysis and forecast, in an

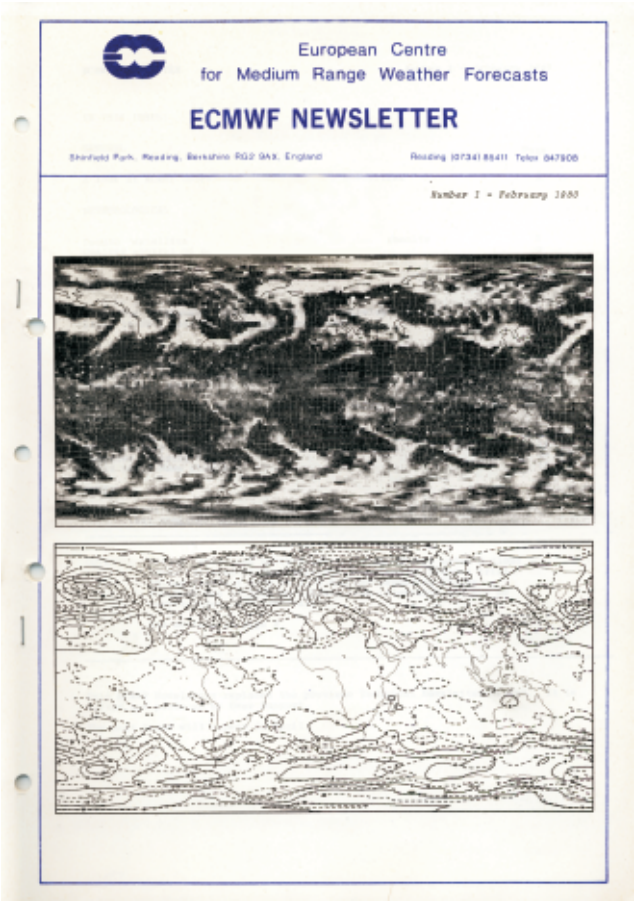
European Centre
for Medium Range Weather Forecasts
ECMWF NEWSLETTER

attempt to improve the quality of the forecasts and overcome some of the known shortcomings. However, in view of the fact that many meteorological services are already now using the Centre's products on a routine basis, the assistance of Member States in identifying problems will be very valuable. With this in mind, a number of additional products, including humidity and vertical velocity, will be released for dissemination in the very near future.

The expected reliability of the forecasting system is another important element, particularly for Member States planning how to use ECMWF products. During the operational testing period the whole system has been encouragingly reliable.

In fact, at the time of writing, only one forecast (17 January 1980 12Z) has been lost since August 1979. In addition some forecasts have been delayed by a few hours. This experience may, perhaps, give a slightly too optimistic view for the future. It should be assumed that at least a few forecasts per month will be lost or seriously delayed because of hardware or software problems at the Centre or problems with the telecommunications links.

Even if operational forecasting is the most important activity of the Centre, and therefore must have higher priority than any other application, only some 50% of the computer resources are normally required for these activities. The rest is to be shared primarily between the Centre's research projects and the Member States, mainly for research in the area of numerical weather prediction. Some problems can be foreseen here in the autumn of this year when daily operational forecasting will have begun and with many Member States having started to use actively the resources allocated to them. At present both the CRAY-1 and the CYBER 175 are already used almost to their full capacity. As it is likely that the research requirements for computer resources will increase rapidly, the problems of allocating and scheduling the available resources will become more serious, and turn-round times will increase.

Finally, I would like to stress two main aspects of ECMWF – operational and international. As already stressed above, the operational routine will have the highest priority, and all efforts will be made to produce forecasts whenever possible; on some days this may mean that the computer system is not available to remote batch users in Member States or users within the Centre. As regards the international aspect, it should be recognised that the majority of the users of our products and services will be found in the Member States.

Daniel Söderman

Monthly Forecasting

Why monthly forecasting? – The monthly forecasting system fills the gap between the two currently operational forecasting systems at ECMWF: medium-range weather forecasting and seasonal forecasting. The monthly forecasting system produces forecasts for the time-range 10 to 30 days; this is probably still short enough that the atmosphere retains some memory of its initial state and it may be long enough that ocean variability has an impact on the atmospheric circulation. Consequently, the monthly forecasting system has been built as a combination of the medium-range ensemble prediction system (EPS) (*Buizza et al.* 2001) and the seasonal forecasting system (*Anderson et al.* 2003a,b). It contains features of both systems and, in particular, is based on coupled ocean-atmosphere integrations, as is the seasonal forecasting system.

An important source of predictability in the monthly time-range over Europe is believed to originate from the Madden-Julian Oscillation (MJO). Several papers have suggested that ocean-atmosphere coupling has a significant impact upon the speed of propagation of an MJO event in the Indian Ocean and the western North Pacific. The use of a coupled system may, therefore, help to capture some aspects of MJO variability.

The monthly forecasting system

The monthly forecasts are based on an ensemble of 51 coupled ocean-atmosphere integrations (one control and 50 perturbed forecasts). The length of the coupled integration is 32 days, and the frequency of the monthly forecasts is currently every two weeks, which is more frequent than for the seasonal forecasting system (once a month) but less frequent than the EPS (twice a day). The atmospheric component is the same as the integrated forecasting system (IFS) with the same cycle as the deterministic forecast. Currently, the atmospheric model is run at T_L159 resolution (1.125° ×1.125°) with 40 levels in the vertical. This represents a resolution in between the EPS ($T_L255L40$) and the seasonal forecasting system (T_L95L40). The oceanic component is the same as for seasonal forecasting system 2 (*Anderson et al.* 2003a,b). It consists of the Hamburg Ocean Primitive Equation (HOPE) model developed at the Max Planck Institute. The ocean model has lower resolution in the extra-tropics but a higher resolution in the equatorial region in order to resolve ocean baroclinic waves and processes, which are tightly trapped at the equator. The ocean model has 29 levels in the vertical. The atmosphere and ocean communicate with each other through a coupling interface called OASIS (Ocean, Atmosphere, Sea-Ice, Soil), which was developed at the Centre Européen de Recherche et de Formation Avancée en Calcul Scientifique (CERFACS). The atmospheric fluxes of momentum, heat and fresh water are passed to the ocean every hour and, in exchange, the ocean sea surface temperature (SST) is passed to the atmosphere. The frequency of coupling is higher than in seasonal forecasting (every 24 hours), since high-frequency coupling may have some impact on the development of some synoptic-scale systems, such as tropical cyclones.

Atmospheric and land-surface initial conditions are obtained from the ECMWF operational atmospheric analysis/reanalysis system. Oceanic initial conditions originate from the oceanic data assimilation system used to produce the initial conditions for the ECMWF seasonal forecasting system. However, the oceanic data assimilation system lags about 12 days behind real-time. In order to 'predict' the ocean initial conditions, the ocean model is integrated from the last analysis, forced by the analysed wind stress, heat fluxes and precipitation-minus-evaporation from the operational analysis. During this 'ocean forecast', the sea surface temperature is relaxed towards persisted SST, with a damping rate of 100 $Wm^{-2}K^{-1}$. This method allows us to produce monthly forecasts in 'real-time' without having to wait for the ocean analysis to be ready.

The monthly forecasting system is run 51 times from slightly different initial conditions. One forecast, called the control, is run from the operational ocean and atmosphere analyses. The 50 additional integrations, the perturbed members, are made from slightly different initial atmospheric and oceanic conditions that are designed to represent the uncertainties inherent in the operational analyses. The atmospheric component of the coupled system is perturbed in the same way as in the EPS for medium-range forecasts. The 50 perturbations are produced using the singular-vector method. These include perturbations in the extratropics and perturbations in some tropical areas by targeting tropical cyclones. In addition, in order to take into account the effect of uncertainties in the model's subgrid-scale parametrization, the tendencies in the atmospheric physics are randomly perturbed during the model integrations. The current implementation is the same as that used in EPS. For each ensemble member, the stochastic physics perturbs grid-point tendencies of the physics by up to 50%. The tendencies are multiplied by a random factor drawn from a uniform distribution between 0.5 and 1.5. The random factor is constant within a 10°×10° domain, for six hours. The whole globe is perturbed. The oceanic initial conditions are perturbed in the same way as in the operational ECMWF seasonal forecasting system.

After 10 days of coupled integrations, the model drift begins to be significant. The effect of the drift on the model calculations can be estimated from integrations of the model in previous years (the back-statistics). The drift is removed from the model solution during the post-processing. In the present system, the model climatology (back-statistics) is deduced from a five-member ensemble of 32-day coupled integrations, starting on the same day and month as the real-time forecast for each of the past 12 years. For instance, if the first starting date of the real-time forecast was 27 March 2002, the corresponding climatology would be derived from five-member ensembles starting on 27 March 1990, 27 March 1991, ..., 27 March 2001. Five-member ensembles are thus integrated with 12 different starting dates. This represents a total of 60 integrations and constitutes the 60-member ensemble of the back-statistics. The size of the back-statistics ensemble (60) is of same order as the size of the real-time forecast ensemble (51). The back statistics are created every two weeks, alternately with the real-time forecast. Figure 1 displays the weekly evolution of the model drift of geopotential height at 500 hPa. During the first weekly period (days 5–11), the drift is relatively small, but increases regularly week by week. The pattern of the model bias in that timescale is consistent with the patterns of the model bias in the seasonal time-range.

Accessing data and products

Monthly forecasting products are displayed on the ECMWF web pages. They include anomaly, probability and tercile maps based on comparing the 51-member ensemble distribution of the real-time forecast with the 60-member ensemble distribution of the model climatology. The forecasts are based on weekly means; fields like surface temperature, 2m temperature,

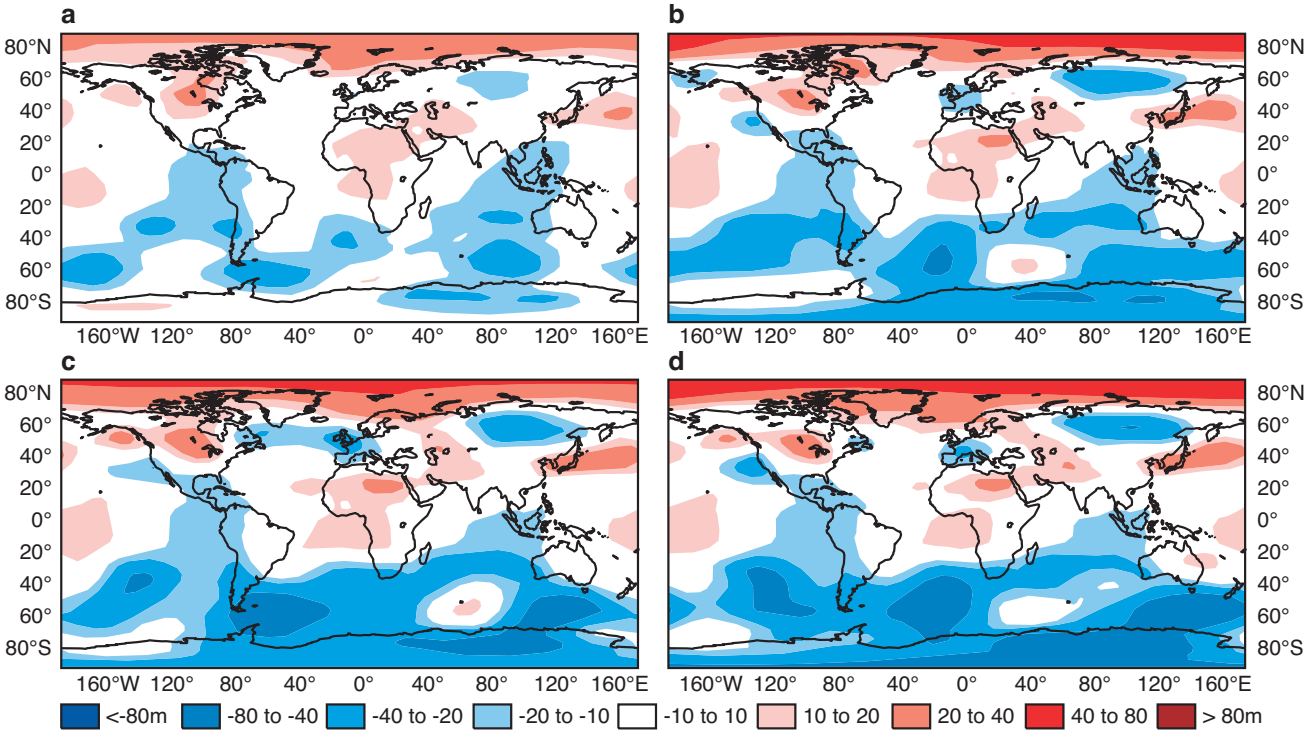

Figure 1 Model bias of the 500 hPa geopotential height for the following periods: (a) days 5–11, (b) days 12–18, (c) days 19–25 and (d) days 26–32. The bias has been computed by taking the difference between the mean of the hindcasts produced for all the real-time forecasts from 27 March 2002 to 17 December 2003 and the corresponding analysis from ERA-40. This figure shows the time evolution of the weekly-mean bias.

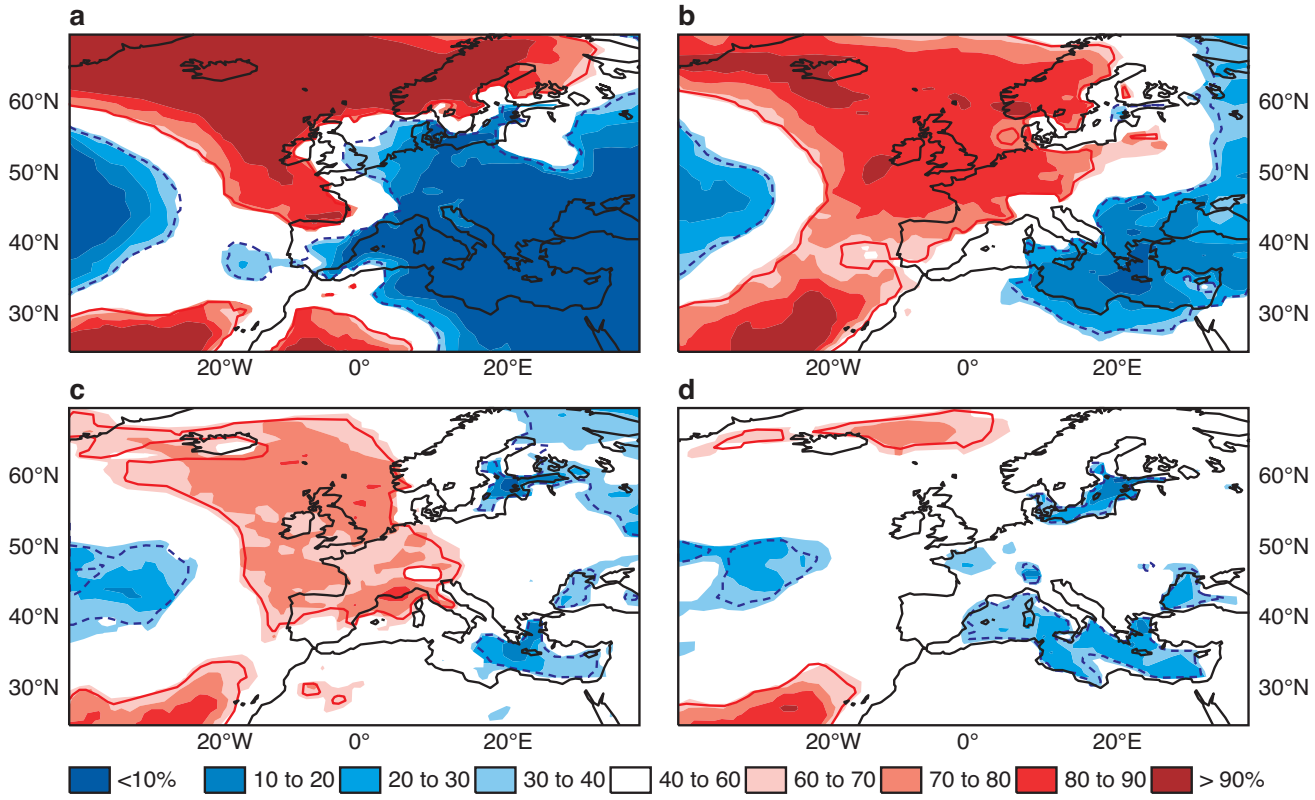

Figure 2 The probability of the 2m temperature anomalies predicted by the monthly forecasting system being greater than zero. Each panel represents one seven-day period: (a) days 5–11, (b) days 12–18, (c) days 19–25 and (d) days 26–32. The forecast starting date is 12 March 2003. The ensemble distribution of the real-time forecast has been compared with the distribution of the model climatology (hindcasts), and a WMW-test has been applied in order to determine if the difference is significant. Areas where the significance is less than 90% have been left blank. This figure shows that the model is drifting towards the model climatology and, in the last period (d), there are few areas where the model predicts a significant anomaly of 2m temperature.

precipitation and mean-sea-level pressure are averaged over seven days. The seven-day periods correspond to days 5–11, days 12–18, days 19–25 and days 26–32. These periods have been chosen so that they correspond to Sunday to Saturday calendar weeks (the monthly forecasting starting date is on Wednesday at 00 UTC). For the purpose of evaluating the skill of extended-range forecasts, this definition has the advantage that the second weekly period is beyond day 10 and corresponds almost to the first week after the 10 days time-range.

The length of the monthly forecasting system is 32 days, so that it contains four of these weekly periods. Figure 2 displays a typical example of a probability map produced by the ECMWF monthly forecasting system. The example displayed in Figure 2 is the probability that the weekly-mean 2m temperature anomalies (relative to the model climatology from the past 12 years) predicted by the monthly forecast starting on 12 March 2003 are positive. A Wilcoxon-Mann-Whitney test (WMW-test) has been applied to estimate whether the ensemble distribution of the real-time forecast is significantly different from the ensemble distribution of the back-statistics. Regions where the WMW-test displays a significance less than 90% have been left blank. In other words, coloured areas in Figure 2 represent areas where the model displays some potential predictability. Unsurprisingly, the percentage of areas that are coloured decreases week by week, indicating that the model drifts towards its climatology. In general the model displays strong potential predictability over a large portion of the extratropics for the period 12–18 days. However, there is generally a sharp decrease of potential predictability in the last two weeks of the forecasts. After 20 days, the ensemble distribution is close to the model climatology. However, there have been several cases, such as the forecast starting on 31 December 2003, where the monthly forecast displayed strong potential predictability in the last two weeks of the forecast period over most of the Northern Hemisphere.

Some EPS products have been extended to the monthly timescale. These include stamp maps of geopotential at 500 hPa and mean-sea-level pressure, plumes and weather regime clusterization. All these products are displayed on the ECMWF web site. Some new products have been created for monthly forecasting: a Hovmöller diagram of geopotential height at 500 hPa and weekly maps of 500 hPa geopotential anomalies.

A brief assessment of performance

Deterministic scores

The ECMWF monthly forecasting system has been run routinely since 27 March 2002. The following sections discuss the verification of 45 real-time cases (between 27 March 2002 and 17 December 2003). The analysis used to

verify the monthly forecasting system is the ECWMF operational analysis or ERA-40 reanalysis (*Uppala et al.* 2004) when available. For precipitation, the operational or the ERA-40 forecasts of precipitation between 12 and 36 hours were used as verification data.

For all 45 cases, the anomaly correlation and root-mean-square (RMS) scores of the ensemble mean have been calculated. Figure 3 displays the daily scores of the ensemble mean for all the 45 cases over the northern extratropics (north of 30°N). Each line represents one individual case, and the red line represents the mean over the 45 cases. An anomaly correlation of 0.6 is reached between day 7 and day 15, and on average at day 8. The linear correlation diminishes quite sharply after day 8 and reaches 0.3 around day 13 on average. The RMS error of the ensemble mean (the red line in Figure 3(b)) reaches climatology around day 14, suggesting that there is little deterministic skill in the monthly forecasting system after about 15 days of forecast.

There is some variability depending on the geographical area. For instance, over Europe, the anomaly correlations decrease much quicker than over the northern extratropics as a whole. The anomaly correlation reaches 0.3 shortly after day 10, and reaches zero after about day 20. The RMS error reaches climatology after just 11 days. Over the North Pacific, on the other hand, the anomaly correlation drops much more slowly with time, reaching 0.3 around day 15 and zero around day 28. The RMS error over the North Pacific reaches climatology around day 18, which is almost one week later than over Europe. There is also some seasonal variability, with summer being a particularly difficult season.

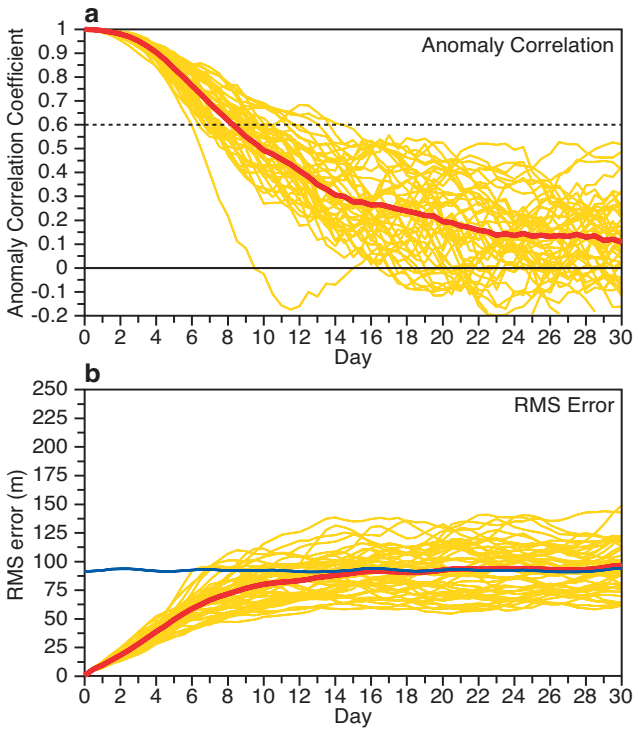

Figure 3 (a) The anomaly correlation and (b) the root-mean-square error of the 500 hPa geopotential height calculated over the ensemble mean. Each yellow line represents the time evolution of the deterministic scores for one individual case (there are 45 real-time cases from 27 March 2002 to 17 December 2003, two weeks apart). The red line represents the mean over all the cases. The blue line in panel (b) represents the root-mean-square error obtained with climatology.

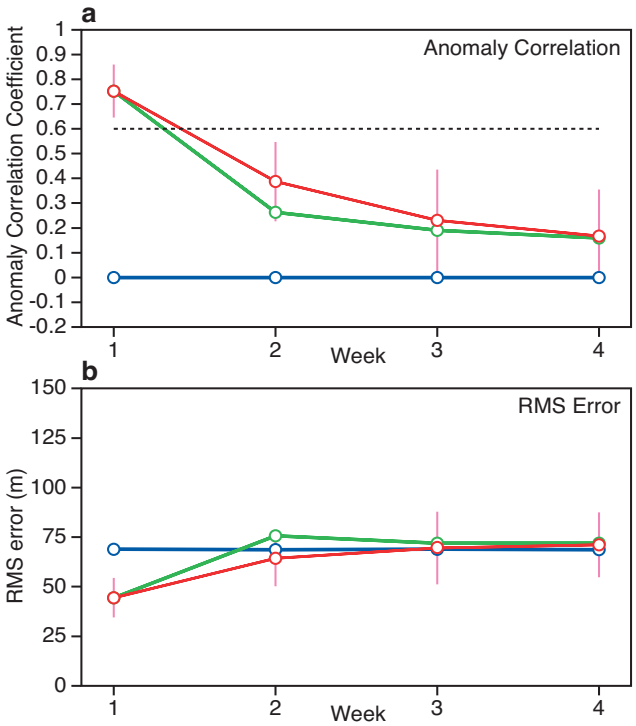

Figure 4 (a) The anomaly correlation and (b) the root-mean-square error of weekly averaged 500 hPa geopotential height calculated over the ensemble mean and averaged over the 45 cases. The red line represents the scores of the monthly forecasting system. The vertical magenta lines represent two standard deviations. The green line represents the scores obtained by persisting the 500 hPa geopotential-height anomaly of the previous week and the blue line represents the scores obtained with climatology.

The anomaly correlations and RMS errors have also been calculated on a weekly-mean basis (Fig. 4). The anomaly correlation is of the order of 0.75 for days 5–11, about 0.35 for the days 12–18, about 0.2 for the days 19–25 and 0.17 for the days 19–32. The RMS error plot suggests that the RMS error of the monthly forecasting system reaches climatology by days 12–18. The anomaly correlations for the three last weekly periods are significantly higher than those obtained by persisting the anomalies of the previous week (the green curve in Fig. 4). This suggests that, although the deterministic skill of the monthly forecasting system is low after 10 days, it is still higher than persistence. This suggests that the monthly forecasting system may be useful at that time-range.

Probabilistic scores

After 10 days, the spread of the ensemble forecast starts to be large, and the forecasts are essentially probabilistic. At that time-range, the probability distribution function provides

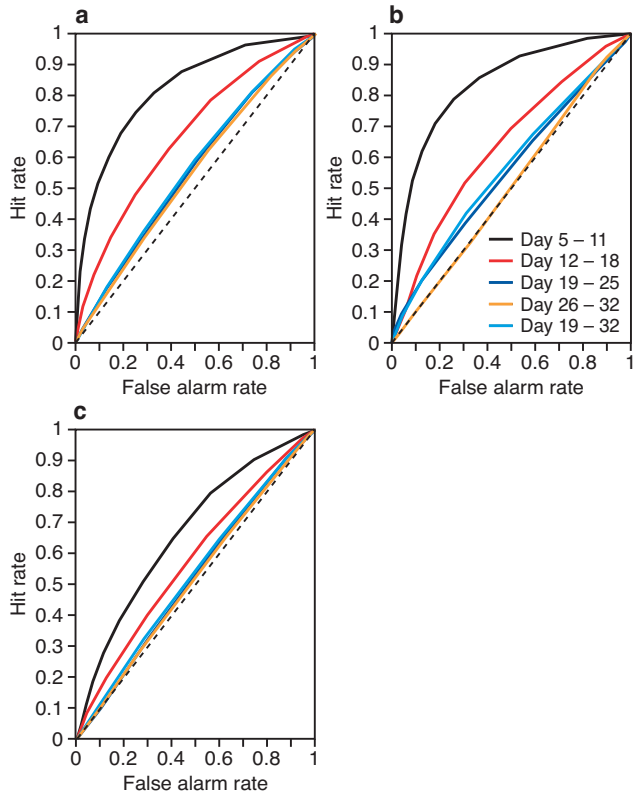

Figure 5 ROC diagrams of the probability that (a) the weekly-mean surface temperature, (b) the precipitation and (c) the mean-sea-level pressure are in the upper tercile. The diagrams have been calculated over all the grid points over the northern extratropics (north of 30°N) and over 45 cases. The solid black line represents 5–11 days, the red line represents 12–18 days, the dark blue line represents 19–25 days, the orange line represents 26–32 days, and the cyan line represents the two-week period 19–32 days.

more information than the ensemble mean. In this section, the probabilistic scores of the monthly forecasting system are evaluated through the scores obtained with weekly averaged surface temperature, 2m temperature, precipitation and mean-sea-level pressure.

Basic methods for verifying probabilistic forecasts have been in use for several years at ECMWF for medium-range EPS products and the methodology is now being naturally extended to monthly forecasts. The Relative Operating Characteristics (ROC) curve shows, for a range of different probability thresholds, hit-rates versus false-alarm-rates of forecasts of a particular event in different regions. Figure 5 displays an example of ROC diagrams obtained with four different periods: days 5–11, days 12–18, days 19–25 and days 26–32. In Figure 5(a) the event scored is the probability that the surface temperature is in the upper tercile over each grid point of the northern extratropics. Only grid points over land are considered. For the monthly forecast, the upper tercile has been computed relative to the model climatology. In that respect, the systematic bias of the model has been taken into account. Figure 5 shows how the probabilistic scores decrease week by week. Over the first period (days 5-11), the ROC score is of order of 0.8, and drops to 0.7 in the next week. It drops again to about 0.6 in the following week. The ROC scores for days 19-25 and days 26-32 are close. For mean-sea-level pressure (Figure 5(b)), the drop between days 5-11 to days 12-18 is larger than with other variables. There is also a significant drop between days 12-18 and days 19-25. For days 26-32, the ROC score is almost 0.5, which suggests that there is almost no skill at that time-range for this variable. The rate at which the ROC score degrades from one week to another depends on the variable considered. For precipitation (Figure 5(c)), the ROC scores are lower than those obtained with the other variables for all the periods, and the ROC score for days 12-18 is about 0.6 only. These results suggest that for days 12-18 the model has some moderate skill, and performs better than climatology. For the two following weeks, the model displays some low skill, but the performance seems generally slightly better than climatology.

Skill of the system for days 12–18

The period 12–18 days corresponds almost to the first week after the end of the ECMWF medium-range forecast. At this time-range the monthly forecasting system still produces a significant signal (see for instance Figure 2(b)). For precipitation, which is a much noisier field than 2m temperature, areas with a significant signal are much smaller than for the 2m temperature.

In order to assess the skill of the monthly forecasting system at that time-range, the ROC score has been computed for each grid point over land on a 2.5°×2.5° grid (Figure 6) over the period March 2002 to December 2003 (45 cases) for the probability that the 2m temperature is in the upper tercile. According to Figure 6, areas where the ROC score exceeds 0.5 (red areas) largely dominate over most regions. This suggests that, according to this test, the model produces better forecasts of the probability that the 2m temperature anomaly is in the upper tercile than climatology for the time-range 12-18 days. The ROC diagram computed over the 45 cases and over all the land points in the whole northern extratropics (north of 30°N) confirms the skill of the model relative to climatology, with a ROC score of 0.67, at least for this particular event and period of verification. The score is, of course, much smaller than the scores obtained in the medium range, when ROC scores are usually larger than 0.8, but it is still significantly higher than 0.5 (the score obtained with a no-skill forecast).

Another way of assessing the skill of probabilistic forecasts is the use of reliability diagrams (*Wilks* 1995). Figure 7 displays the reliability diagram of the probability that the 2m temperature averaged over days 12–18 is in the upper tercile. This graph displays the observed frequency as a function of the forecast probability. The fact that the reliability graph in Figure 7 is flatter than the 45° diagonal suggests that the model is overconfident; low risks are underestimated and high risks are overestimated. The Brier skill score is positive (0.04), indicating that the model is more reliable than climatology. The distribution of model probabilities for 12–18 days presents a maximum around the climatological probability and decreases

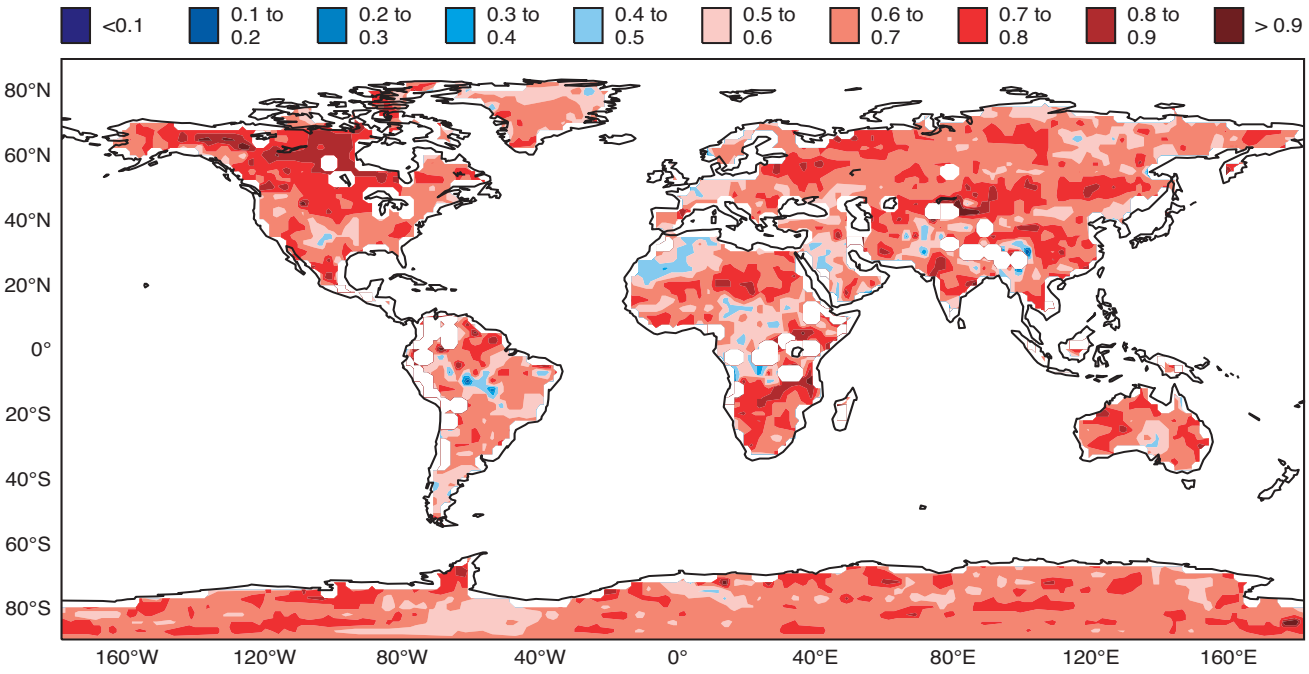

Figure 6 Map of ROC scores of the probability that the 2m temperature is in the upper tercile (defined from the model climatology) for days 12-18. Only the scores over land points are shown. The verification period is March 2002 to December 2003. The red corresponds to ROC scores higher than 0.5 (better than climatology) and the blue corresponds to ROC scores lower than 0.5 (worse than climatology).

towards high or low probabilities (circles in Figure 7). In the medium range, the distribution of forecast probabilities presents generally a maximum for very high or low probabilities. Therefore, the forecasts for the time-range 12–18 days have a poor resolution in comparison with medium-range forecasts.

These results suggest that the model performs generally better than climatology for days 12–18. However, for that time-range, comparing the performance of the forecast with the persistence of medium-range forecasts is a much tougher test, as discussed at the beginning of this article. Therefore, in the rest of this section, the scores of the monthly forecast over the period 12–18 days are compared with the persistence of the probabilities of the previous weekly-mean anomalies (days 5–11). It is also possible to persist the ensemble mean of the day 5–11 anomalies instead of persisting the probabilities. However, the ROC scores obtained by persisting probabilities are higher than those obtained by persisting the ensemble mean (not shown), suggesting that comparing the monthly forecasts with the persistence of the probabilities from the previous week is a tougher test than comparing it with the persistence of the ensemble mean of the previous week.

Figure 8(a) shows a comparison of the ROC diagram obtained with the monthly forecasting system for days 12–18 and the probability that the 2m temperature is in the upper tercile (red line) with the ROC diagram obtained when persisting the 2-m temperature anomalies of the previous week (blue line) (this is indeed close to the score obtained by persisting the last week of the EPS). Figure 8(a) suggests that the monthly forecasting system performs better than persistence of the previous week. The ROC score is higher (0.67 instead of 0.61) with the monthly forecasting system than when using persistence. A scatter-plot diagram of each individual case (Figure 9) indicates that the monthly forecasting system outperforms the persistence of the probabilities from the previous week in 70% of cases. A WMW-test suggests that the scores of the monthly forecasting system

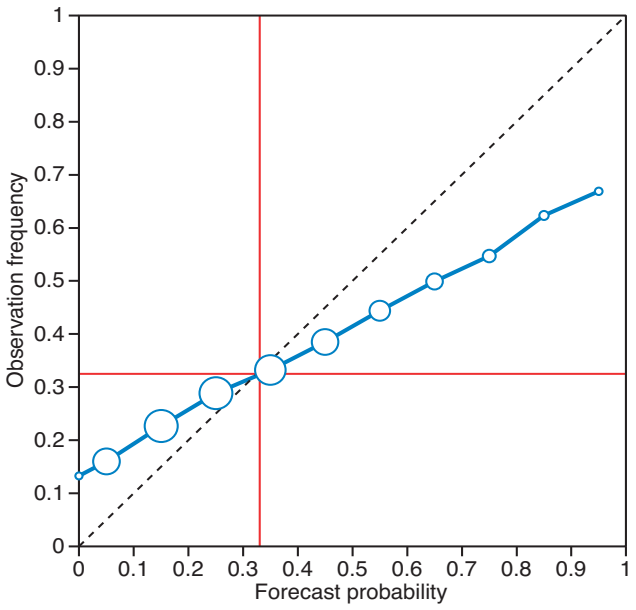

Figure 7 Reliability diagram of the probability that the 2-m temperature averaged over days 12–18 is in the upper tercile. Only land points in the northern extratropics are considered. The size of the circles on the reliability curve is proportional to the population of the forecast-probability bin.

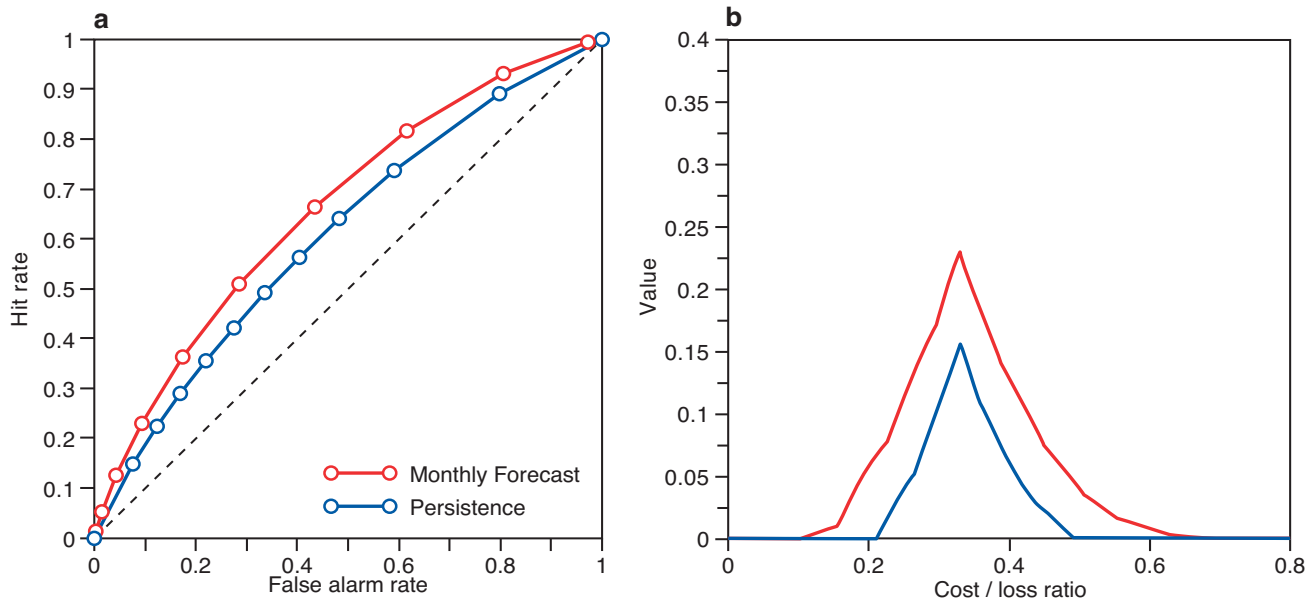

Figure 8 (a) The hit/false-alarm rate and (b) the potential-economic-value diagrams of the probability that the 2m temperature averaged over days 12–18 is in the upper tercile. The red curve represents the results obtained with the monthly forecasting system (ROC score 0.67), and the blue curve the results obtained by persisting the probabilities from the previous week (days 5–11) (ROC score 0.61).

are significantly higher than those obtained with persistence, with a level of confidence larger than 95%. Therefore, the difference in ROC scores presented in Figure 8(a) is likely to be significant. A scatter-plot diagram of Brier skill score indicates an even larger difference between the monthly forecast and persistence; persistence outperforms the monthly forecast in only one case in 45.

To address the potential benefit of the monthly forecasting system to different users, value diagnostics have been calculated, derived from a simple cost-loss model of economic decision-making (*Richardson* 1998). The value V of the monthly forecast is defined as the savings made by using the monthly forecasting system as a fraction of the potential savings that would be achieved with perfect forecast information. $V = 0$ indicates that the forecast has no more value than climatology. In the potential-economic-value diagram, V is a function of the user's cost-loss ratio. Figure 8(b) displays the potential-economic-value diagram obtained with the monthly forecasting system (red curve) for days 12–18, and the potential-economic-value diagram obtained by persisting the probabilities from the previous week (blue curve). The event scored is still the probability that 2m temperature is in the upper tercile. All land points over the northern extratropics for the 45 cases have been taken into account. Figure 8(b) confirms that the monthly forecasting system has some value for a large range of cost-loss ratios, and that it has more value than persisting the probabilities from the previous week.

The fact that the monthly forecasting system produces better forecasts than persistence for days 12–18 is valid for other variables and thresholds. For precipitation (not shown), the ROC scores are higher for the monthly forecasting system than for persistence, although the ROC score (0.58) is much lower for precipitation than for the 2m temperatures. The monthly forecasts of precipitation are more reliable than persistence, with a positive Brier skill score, suggesting that the model performs better than climatology. The difference in scores between monthly forecasts and persistence is even larger with mean sea-level pressure than with 2m temperature. The monthly forecasts of mean-sea-level pressure display strong reliability with, once again, a positive Brier skill score, whereas the persistence of the previous week shows a poor reliability, with a reliability diagram close to the horizontal line and a negative Brier skill score of –0.29. Scatter-plot diagrams indicate that the difference between scores for monthly forecasts of mean-sea-level pressure and for the persistence of the probabilities from the previous week (days 5–11) is significant, with a level of confidence larger than 95%. Persistence outperforms the monthly forecasting system on only a few occasions. All these results indicate that, overall, the monthly forecasting system outperforms persistence and climatology over the northern extratropics, suggesting that it produces useful forecasts for days 12–18.

However, the performance varies from one region to another. The model is particularly skilful over North America (ROC score of 0.7 and the ROC score of persistence is 0.6). Over the southern extratropics (south of 20°S) the scores are about the same as over the northern extratropics. Over the tropics the model displays less skill, but still performs better than persistence of the probabilities from the previous week. Europe is a more difficult region. Over Europe, the potential economic value is much less than over the other regions, and the scores based on all the land points over Europe are not significantly better than those based on persistence of the previous week's anomalies.

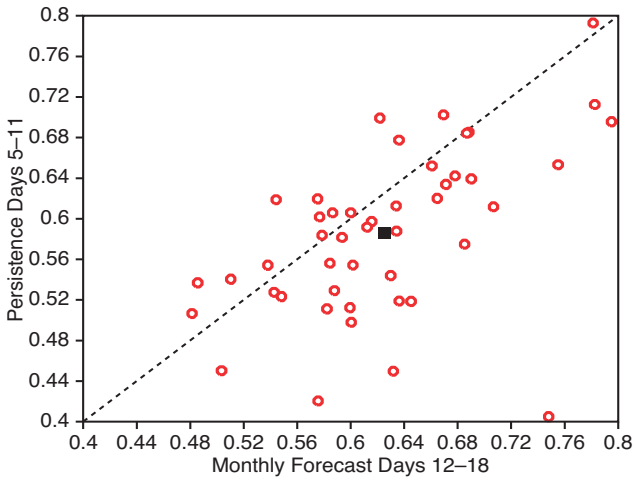

Figure 9 Scatter-plot diagram of ROC scores of the probability that the 2m temperature averaged over days 12–18 is in the upper tercile. The x-axis represents the scores of the monthly forecasting system, and the y-axis represents the score of the forecast obtained by persisting the anomaly forecasts of the previous week (days 5–11). Each red circle represents one case (of a total of 45). The square represents the mean of the 45

Skill of the system for days 19–32

The different fields (2m temperature, precipitation, mean-sea-level pressure...) have been averaged over days 19–32 (the two last weeks of the monthly forecast). Brier skill scores, ROC scores, potential economic values have been computed over land grid points for the 45 cases. The scores have also been compared with the scores obtained by persisting the probabilities of the two previous weeks of the forecast (days 5–18), so that the period persisted has the same length as the forecasting period.

The point map of ROC scores for the probability that the 2m temperature anomalies are in the upper tercile (Figure 10) suggests that, over the vast majority of land points, the ROC score exceeds 0.5. This suggests that the model performs better than persistence. However, the scores are generally much lower than those obtained over days 12–18 (Figure 6). The ROC score calculated over all the grid points in the northern extratropics is slightly better than persistence (Figure 11(a)). This difference seems to be significant within the 10% level of confidence according to the WMW-test applied to the ensemble of 45 cases. The model outperforms persistence in 34 cases (Figure 12). This suggests that, over the whole northern extratropics, the model displays moderate skill in predicting the probability that 2m temperature is in the upper tercile, and it performs better than persistence or climatology.

As for days 12-18, there is a strong regional variability and Europe is a particularly difficult region, with a ROC score of about 0.5 (Figure 11(b)). On the other hand, the model displays some skill over North America (Fig. 11(c)), where it performs significantly better than climatology and persistence. Over the tropics and southern extratropics, the conclusions are about the same as for the northern extratropics. After about 20 days, the value of the forecast is very dependent on the threshold of the event. For small thresholds, such as the probability that the 2m temperature anomaly is larger than zero, the potential economic value is quite low, and the model does not perform significantly better than persistence. However, for higher thresholds, for example the probability that the 2m temperature anomaly is larger than 2 K, the model displays some values for lower cost-loss ratios, which exceed the value for persistence (not shown). This suggests that, even at this time-range, the monthly forecasting system could still be useful.

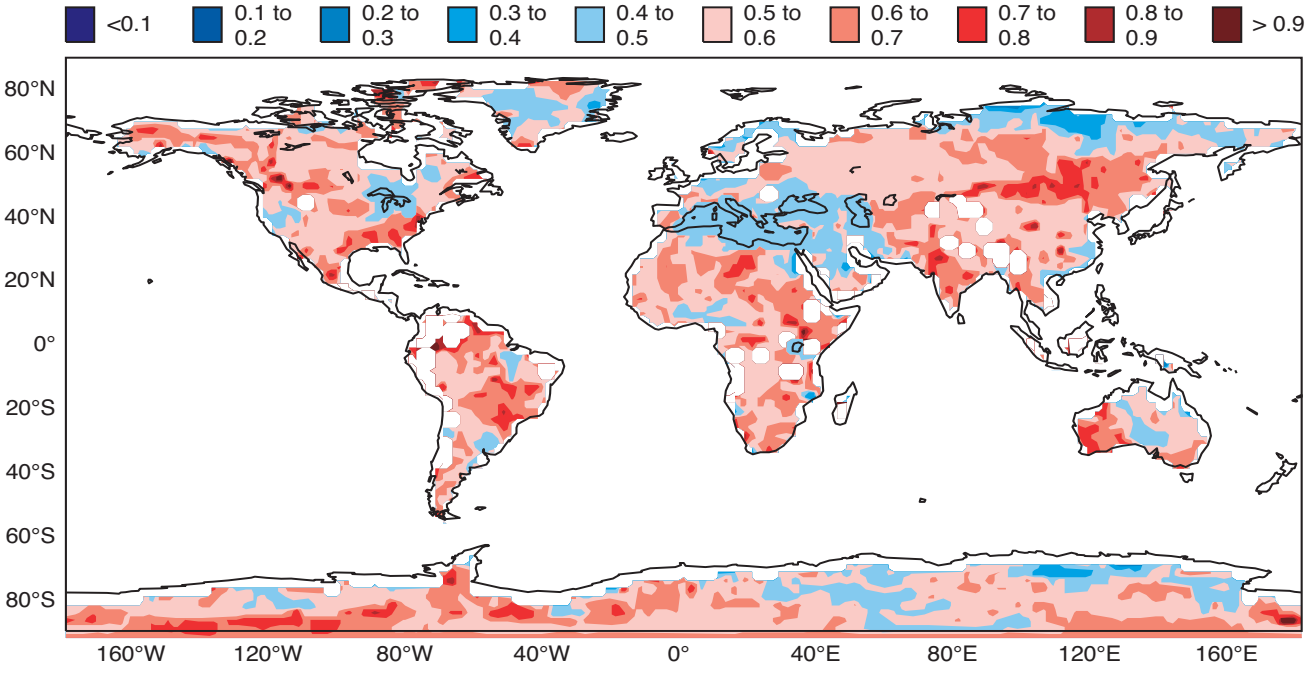

Figure 10 As Figure 6, but for the 2m temperature averaged over days 19-32.

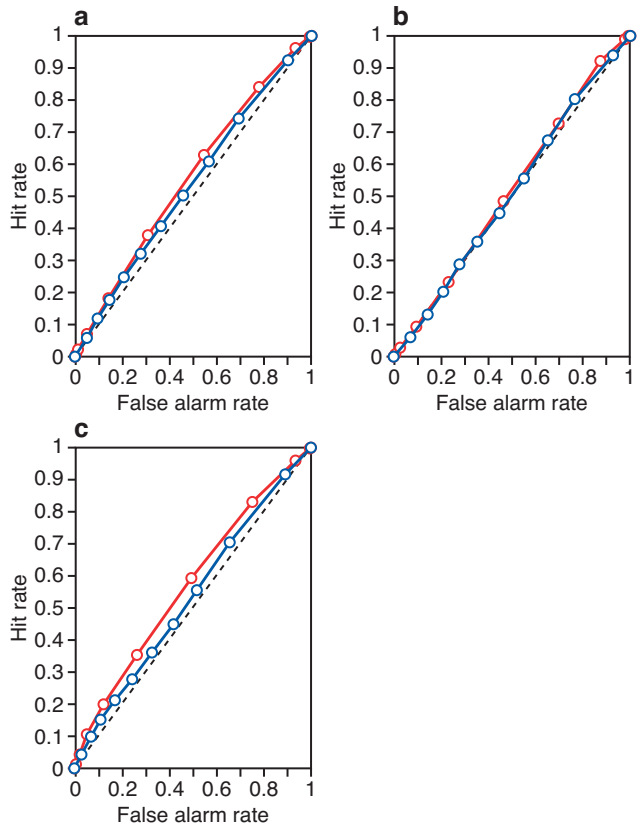

Figure 11 Hit/false-alarm rates of the probability that the 2m temperature averaged over days 19–32 is in the upper tercile over (a) the northern extratropics, (b) Europe and (c) North America. The red curves represent the results obtained with the monthly forecasting system (ROC scores (a) 0.56, (b) 0.5 and (c) 0.57), and the blue curves represent the results obtained by persisting the probabilities from the previous two weeks (days 5–18) (ROC scores (a) 0.53, (b) 0.5 and (c) 0.52).

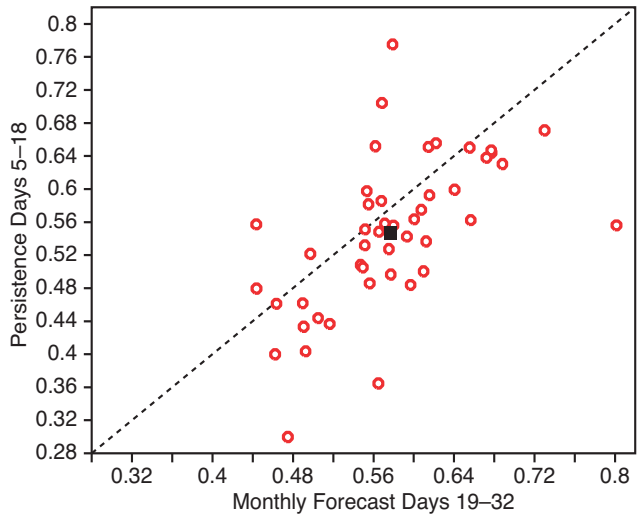

Figure 12 As Figure 9, but for ROC scores of the probability that the 2m temperature averaged over days 19–32 is in the upper tercile. The y-axis represents the score of the forecast obtained by persisting the anomaly forecasts of the previous two weeks (days 5–18).

For surface temperature, precipitation and mean-sea-level pressure, the conclusions are about the same as for 2m temperature. The model displays low skill at this time-range, but still performs slightly better than climatology and persistence of the forecast probabilities from the past two weeks.

Seasonality

In addition to the real-time forecast, a five-member hindcast is produced every two weeks in order to evaluate the model drift and to calibrate the real-time forecast. After more than one year of operations, this represents more than 500 cases spanning over 12 years. ROC scores have been computed for each individual season during the whole

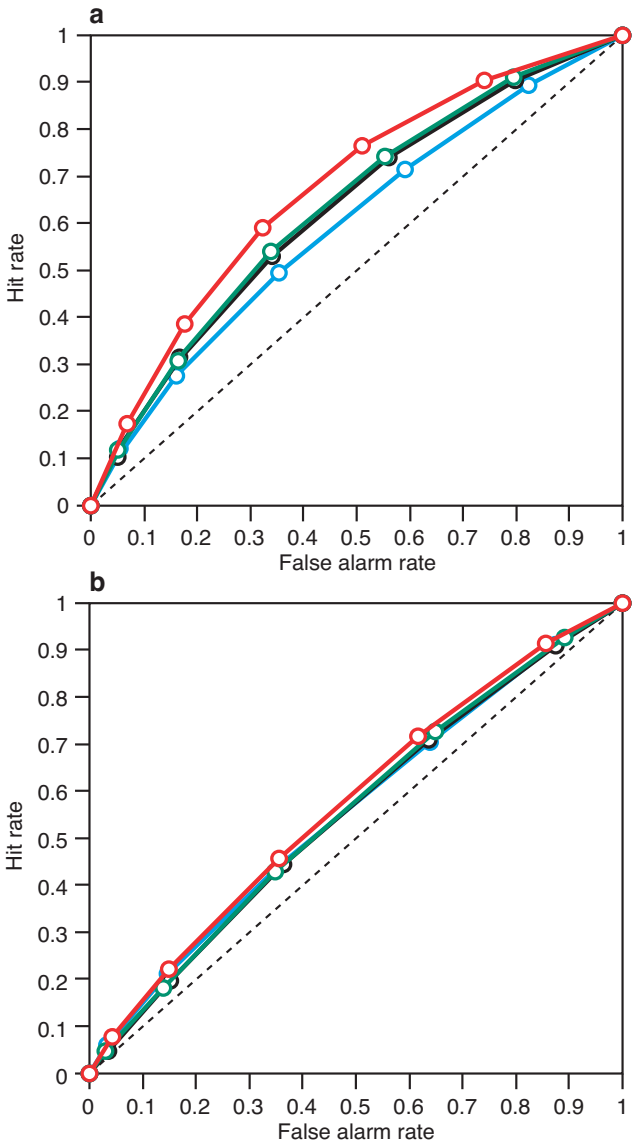

Figure 13 Hit/false-alarm rate diagrams of the probability that the 2m temperature averaged over (a) days 12–18 and (b) days 19–32 is in the upper tercile over the northern extratropics. The red curve represents the scores for winter, the green curve for spring, the black curve for summer and the cyan curve for autumn. The scores have been computed from the five-member ensemble hindcasts from 1991 to 2002.

period of the hindcast for the monthly forecasts and for the persistence of the previous week's probabilities. Figure 13 displays the ROC diagrams for each season for the probability that 2m temperature is in the upper tercile in the northern extratropics. Results for other events suggest that the seasonality does not depend on the event considered. There is a strong and significant seasonality in the probabilistic scores for the period 12–18 days (Figure13(a)). Over the northern extratropics, the ROC score is the highest in winter. Summer is a particularly difficult season, with a ROC score of only 0.59 compared with 0.67 in winter. This result is consistent with the seasonality of the scores in medium-range weather forecasts, where summer is the most difficult season. Winter is not the most persistent season and it is the season where there is the strongest difference between the scores of the monthly forecasting system and the scores of persistence, making it the season where the monthly forecasting system is likely to be the most useful. In spring, the scores of the monthly forecasting system are also significantly higher than the scores of persistence. In summer and autumn, the scores of the monthly forecasts are slightly higher than persistence, making the monthly forecasts during these seasons less useful than in winter or spring. For the southern extratropics (not shown) the results are about the same, with the model displaying the strongest skill during the Southern Hemisphere winter.

During the two last weeks of the forecast, the scores display less seasonality than for the period 12–18 days (Figure 13(b)). Winter still appears to have the highest scores, but the difference from the other seasons is small. The difference for persistence is also strongest in winter. This is also true for the southern hemisphere (not shown).

Example: The heat wave over France in August 2003

The heat wave during the first two weeks of August 2003 was particularly intense, with catastrophic consequences (*Grazzini et al.* 2003) The present study focuses on the week from 3–9 August, when 2m temperature anomalies relative to the past 12-year climate were close to 10 K over some parts of France (Figure 14 (a)). Figure 14(b) displays the monthly forecast starting on 30 July 2003, and shows the ensemble mean of the 2m temperature anomalies (relative to the model climatology) for days 5–11. At that time-range, the model predicted a strong positive anomaly of the 2m temperature, although the intensity of the ensemble mean is less than in the analysis (Figure 14 (a)). Almost all the ensemble members predicted

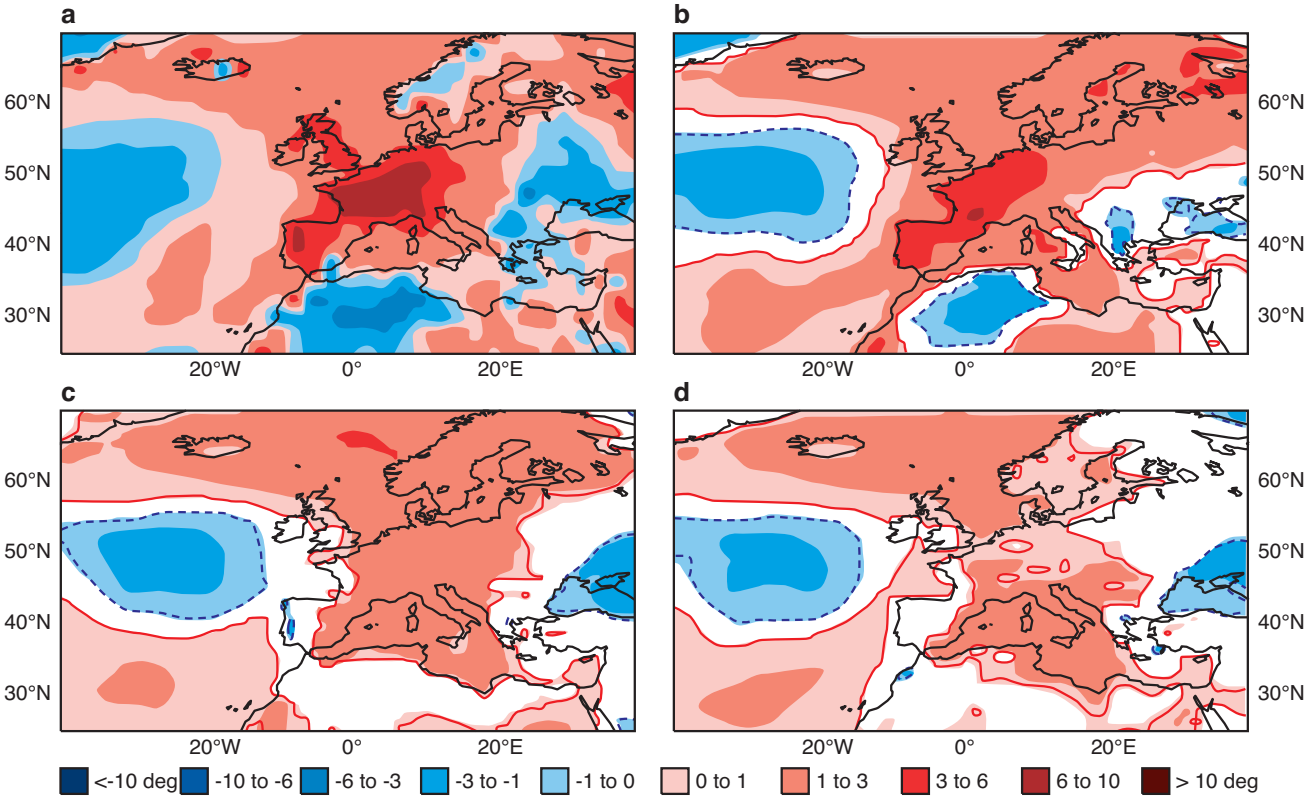

Figure 14 (a) The 2m temperature anomalies for the ECMWF operational analysis (relative to the past 12-year climate computed from the ERA-40 and operational analyses) averaged over the period 3–9 August (the verification). (b) The ensemble mean of the 2m temperature anomalies from the monthly forecasts starting on 30 July 2003 (the 2m temperature anomalies have been averaged over days 5–11 and are relative to the model climatology) – only areas where there is a significant difference between the ensemble distribution of the real-time forecast and the model climatology according to the WMW-test are shown coloured. (c) The 2m temperature anomalies from the hindcast starting on 25 July 2003, and averaged over all the ensemble members and the period days 12–18. (d) The 2m temperature anomaly from the monthly forecast starting on 16 July 2003, and averaged over all the ensemble members and the period days 19–25.

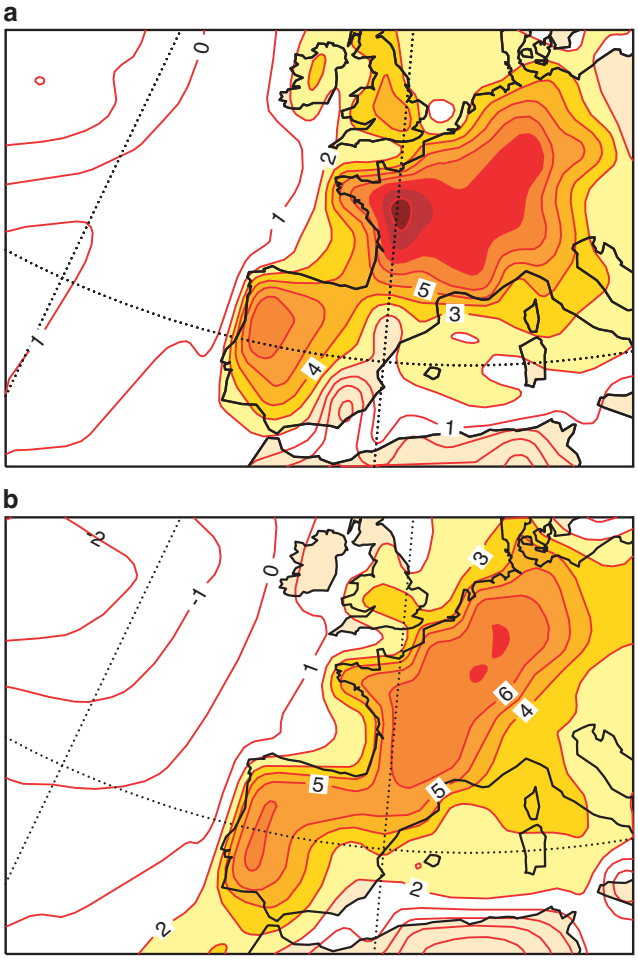

Figure 15 The 2m temperature anomalies averaged over the period 3–9 August. (a) The 2m temperature anomaly from the ECMWF operational analysis. (b) The 2m anomaly predicted by one member of the ensemble (ensemble member 2) and starting on 25 July 2003. The contour interval is 1 K. Areas where the anomaly exceeds 2 K are coloured. This figure indicates that some members of the ensemble predicted a significant heat wave over Europe more than ten days in advance.

a significant heat wave, but only a few members of the ensemble predicted an intensity as strong as in the analysis.

The monthly forecasting system runs every two weeks, but for this test case a hindcast starting on 25 July 2003 has been produced to evaluate the weekly evolution of the forecast. A subjective test suggests that fifteen members of the ensemble predict a weekly 2m temperature anomaly larger than 3 K over most of Europe. Four ensemble members display an anomaly with an amplitude of the same order as in the analysis. Figure 15 displays the 2m temperature anomaly over Europe predicted by one of these ensemble members. In the 60-member ensemble-model climatology corresponding to this real-time forecast, only four members display a weekly 2m temperature anomaly larger than 3 K, and none of them has an amplitude comparable to the analysis. This suggests that, although most ensemble members do not predict a significant heat wave over Europe for days 12-18, the model predicted a probability for this extreme event higher than in the model climatology. The ensemble mean (Figure 14(c)) displays a significant and positive anomaly in the 2m temperature averaged over days 12-18 over most of Europe. However, since the anomaly is averaged over all the ensemble members, its magnitude is less than in the analysis.

Stamp maps for days 19-25 of the monthly forecast starting on 16 July 2003 indicate that 12 ensemble members predict a weekly 2m temperature anomaly larger than 3 K, with one forecast displaying a positive 2m temperature anomaly as strong as in the analysis. In the model climatology corresponding to this forecast, only four ensemble members display a weekly 2m temperature anomaly larger than 3 K, and none of them has an amplitude comparable to the analysis. This suggests that, 20 days in advance, the model predicted a higher probability than usual of a significant heat wave over Western Europe. The ensemble mean (Figure 14(d)) displays a strong and significant (although weaker than in the analysis) positive anomaly over a large portion of Europe. Such a strong signal in the ensemble mean is quite unusual for this time-range.

Plans for operational production

Currently the monthly forecasting system is run once every two weeks and is still experimental and under technical development. It is planned to run the system operationally once a week with product generation by summer 2004. Product dissemination is expected to become available later in the year.

Acknowledgements

We acknowledge input from everyone in the Seasonal Forecasting Section and the substantial work by the Meteorological Applications and Operations Sections in implementing the new monthly forecasting system.

FURTHER READING

Anderson, D., T. Stockdale, M. Balmaseda, L. Ferranti, F. Vitart, P. Doblas-Reyes, R. Hagedorn, T. Jung, A. Vidard, A. Troccoli and **T. Palmer**, 2003a: 'Comparison of the ECMWF seasonal forecast systems 1 and 2, including the relative performance for the 1997-1998 El Niño'. *ECMWF Technical Memorandum,* **404**
http://www.ecmwf.int/publications/ library/do/references/list/14

Anderson, D., T. Stockdale, L. Ferranti and **M. Balmaseda**, 2003b: The ECMWF seasonal forecasting system. *ECMWF Newsletter,* **98**, 17–25

Buizza, R., D.S. Richardson and **T.N. Palmer**, 2001: The new 80-km high-resolution ECMWF EPS. *ECMWF Newsletter*, **90**, 2–9

Grazzini, F., L. Ferranti, F. Lalaurette and **F. Vitart**, 2003 The exceptional warm anomalies of summer 2003. *ECMWF Newsletter*, **99**, 2–8

Richardson, D.S., 2000: Obtaining economic value from the EPS, 1998: *ECMWF Newsletter*, **80**, 8–12

Uppala, S., *et al.* 2001: ECMWF Re-Analysis 1957-2001, ERA-40. *ECMWF Newsletter*, **100**,

Wilks, D.S., 1995: Statistical methods in the atmospheric sciences: An introduction. *Academic Press*

Frederic Vitart

Systematic errors in the ECMWF forecasting system

The aim of ECMWF is to carry out medium-range, monthly, and seasonal forecasts using numerical models of the atmosphere and ocean. Uncertainties in the initial conditions, or analyses, as well as model deficiencies lead to the development of forecast errors. The time dependent forecast error can be expressed as the difference between the forecast and our best estimate of the truth (e.g., the analysis). Continuous monitoring at ECMWF reveals that forecast errors have been substantially reduced in recent years, particularly in the medium-range. This reduction of forecast errors is partly due to improved initial data and partly due to model improvements. In general, however, it is not straightforward to separate the influence of improved analyses from those due to improved model formulations, since models are used in data assimilation schemes to determine the analysis.

A relatively simple way to identify model error is to focus on systematic errors of the forecast. To this end, a particular meteorological aspect (e.g. the mean circulation) is quantified from a large set of forecasts. The model results are then compared with estimates of the truth, which are obtained from observational data (or analyses). The ability of this technique to isolate model error depends on three factors. Firstly, it is assumed that the influence of possible systematic errors in the initial conditions is negligible. This assumption seems reasonable given the relatively short adjustment time scale of the atmosphere; the model 'forgets' about the initial bias during the course of the integration. Secondly, estimates should be based on large samples. To illustrate this point consider one month of daily D+10 forecasts of Northern Hemisphere 500 hPa geopotential height fields (Z500). If this month was characterized by weak, westerly winds then this is reflected in the observations. Further, suppose that predictability has been lost at D+10 in this particular month. Then, even for a perfect model, differences in the strength of the westerlies between the forecast and observations are likely to wrongly suggest that the model has a westerly wind bias. Finally, the observational data set used as truth might be biased. While this is less likely to be the case for Z500, existing precipitation climatologies, for example, are associated with considerable uncertainties.

At the beginning of 2003 it was decided to carry out a comprehensive study of systematic error in the ECMWF forecasting system. This decision was motivated by the fact that such a systematic major documentation had not been carried out for some time and that the ECMWF model underwent considerable improvements in recent years (e.g. *Andersson et al.* 2003). In the following, we describe some of the key results of this study. The following questions are addressed:

- What are the major systematic errors in the latest ECMWF model cycles?
- How do systematic model errors grow from the medium-range to the extended-range?
- How have systematic errors evolved over the years?

Readers who are interested in a more detailed survey are referred to the paper by *Jung and Tompkins* (2003).

Strategy

It seems reasonable to expect that systematic errors grow during the course of the integration, thereby changing their magnitude as well as their spatial structure. Therefore systematic errors should be separated into two components, transient and asymptotic. Asymptotic systematic errors describe errors that are associated with the model's own climate. Here, they are obtained from a set of seasonal six-month integrations with an atmospheric-only model discarding the first two months during which most of the systematic error growth takes place.

The main model cycle used to describe asymptotic systematic errors is 26r1 at resolution of T_L95L60 (Table 1). This cycle was operational from 29 April to 6 October 2003.

Most of the transient growth takes place in the short-medium range. Transient systematic errors along with their evolution over the last 20 years are studied using operational medium-range forecasts. In order to diagnose systematic model error beyond D+10, operational control forecasts from the ECMWF Ensemble Prediction System (EPS), which are carried out to D+20, are additionally used.

As mentioned above, it is necessary to use large samples to reliably estimate systematic model errors. Given that the ECMWF model is changed at regular intervals (e.g. three different cycles were used in 2003), systematic error estimates usually reflect model errors from more than one cycle. To overcome this problem, medium-range forecasts at a resolution of T_L159L60 (cycle 23r4), which were carried out every day during the period 1960-2001 in the framework of the ERA-40 project, were diagnosed as well. Cycle 23r4 is one of the principal releases of the ECMWF model, forming the atmospheric component of the currently operational seasonal forecasting system (system 2 and DEMETER), in addition to the ERA-40 project (Table 1).

This article first describes systematic model errors of the atmospheric circulation and then the capability of the ECMWF model to simulate synoptic-scale variability is assessed. We then discuss Euro-Atlantic blocking and tropical intraseasonal variability followed by a description of systematic errors of modelled clouds and cloud-related parameters. Finally, it is shown that the use of an improved aerosol climatology substantially reduces many of the systematic errors.

Cycle	Resolution	Operational	Comments
23r4	T_L159L60	12/06/01 – 21/01/02	Used in ERA-40 and seasonal forecasting (system 2)
26r1	T_L95L60	29/04/03 – 06/10/03	Seasonal runs with prescribed SST, 1962–2001
26r3	T_L95L60	07/10/03 – 08/03/04	Seasonal runs with prescribed SST, 1962-2001

Table 1 Some features of the three model cycles used within this study.

Mean atmospheric circulation

A basic requirement for a model used to carry out weather forecasts is that the mean atmospheric circulation is correctly simulated. Here, we focus on the capability of the ECMWF model to simulate Northern Hemisphere Z500 fields during wintertime (December–March). Asymptotic systematic Z500 errors for the period 1962-2001 are shown in Figure 1. A strong anticyclonic bias has developed over the North Pacific after more than two months into the integration resulting in an excessively weak westerly flow in the mid-latitude North Pacific. This bias, which has been already present in earlier model cycles, used to be accompanied by a strong westerly wind bias in the North Atlantic. Evidently, recent model improvements have substantially reduced systematic Z500 errors in the North Atlantic region.

The medium-range forecasts for the period 1960-2001 were analysed to document how Z500 errors develop and whether the North Pacific bias affects the medium-range (Figure 2). It is evident that the most pronounced systematic Z500 errors occur over North America, the North Pacific, and northeast Asia; in the North Atlantic region and over Europe, on the other hand, systematic Z500 errors are small. The rate at which systematic Z500 grow is different from region to region. The positive bias over central North America, for example, grows more or less linearly during the first five days, thereafter it saturates, and by D+10 it is of minor importance. Finally, the spatial structure of systematic Z500 error undergoes some changes during the first ten days of the integration.

A comparison between Figure 1 and 2 shows that by D+10 the positive Z500 bias over the North Pacific has developed to about half its asymptotic size. This suggests that its growth continues well beyond the medium range. To substantiate this conjecture and to further quantify growth characteristics of systematic Z500 errors, 20-day-long control

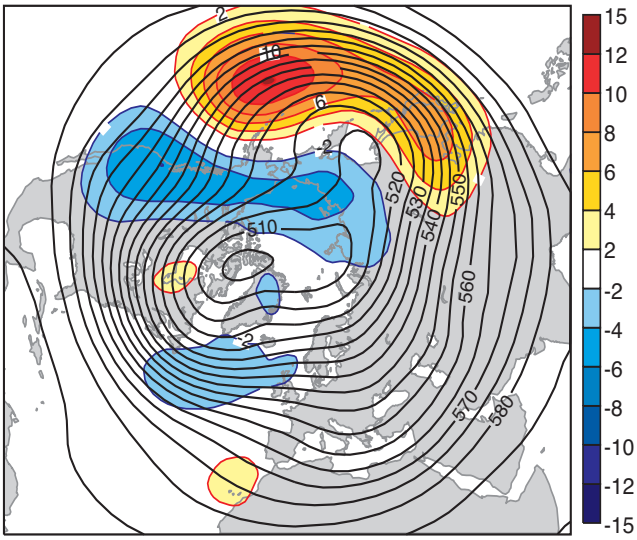

Figure 1 Asymptotic systematic Z500 error (shading in dam) for model cycle 26r1 for winters (DJFM) of the period 1962-2001. Seasonal forecasts were started on 1 October of each year. ERA-40 data has been used as the truth. Also shown is the mean Z500 field obtained from ERA-40 data (black contours).

forecasts from the EPS were diagnosed for winters of the period 2000-2003. The magnitude (expressed in terms of spatial standard deviation) of systematic Z500 errors is shown in Figure 3(a) for different domains and forecast steps (D+1 to D+20). In the North Atlantic region the largest growth takes place during the first six days of the integration; in contrast, the largest growth over the North Pacific takes place beyond D+10. As a consequence, systematic Z500 errors beyond D+10 are much larger in the latter region.

From Figure 2 it appeared that the spatial structure of systematic Z500 errors undergoes substantial changes during the initial days of the integration. This is further quantified in Figure 3(b) showing squared spatial correlation coefficients between systematic Z500 error fields at D+3 and all other forecast steps for different regions. Results are based on 20 day EPS control forecasts. Obviously, there is a striking difference between the northern and southern hemisphere, namely spatial patterns of systematic Z500 error undergo much less spatial changes in the southern hemisphere than their Northern Hemisphere counterparts. Note that, in the Northern Hemisphere, systematic-error fields at D+10 are almost orthogonal to those at D+3, particularly in the North Pacific region.

The next question addressed is how systematic Z500 errors evolved over the years. To this end, next, systematic Z500 errors during wintertime are considered for operational D+3 and D+10 forecasts for the period 1986-88, 1993-95, and 2001–03 (Figure 4). Evidently, the latest model cycles show the lowest systematic Z500 errors at D+3. At D+10, however, the largest systematic-error reduction seems to have taken place between the 1980s and 1990s. Moreover, in some regions the structure of the systematic Z500 error has hardly changed since the 1980s; this is particularly evident in the North Pacific region. The results for the North Atlantic region, however, imply that the systematic Z500 errors have changed from one period to the other. It should be kept in mind, though, that the North Atlantic region has been characterized by pronounced decadal-scale Z500 variability during the periods considered, suggesting that at least some of the 'systematic error' could be due to a small sample size.

A clearer picture of the temporal evolution of the magnitude of the Northern Hemisphere systematic error of operational Z500 forecasts at D+1, D+3, and D+10 can be obtained from Figure 5 showing the reduction compared to the period 1981–83. The largest reduction took place during the early and mid-1980s. However, the reduction during the last 15 years has still been substantial. Overall, the magnitude of systematic Z500 errors over the Northern Hemisphere of recent model cycles has been reduced by 60–70% compared with those seen for model cycles used during the early years of ECMWF.

The results above show that systematic Z500 errors over the Northern Hemisphere are still present in the latest model cycles. Is the magnitude of these errors such that they matter? Evidently, the answer to this question depends on the forecast range and the region being considered. Moreover, the answer to this question also depends on user requirements. In the remainder of this section we try to shed some light on this issue by addressing the following question: If systematic Z500 errors could be removed, would this lead to better forecasts?

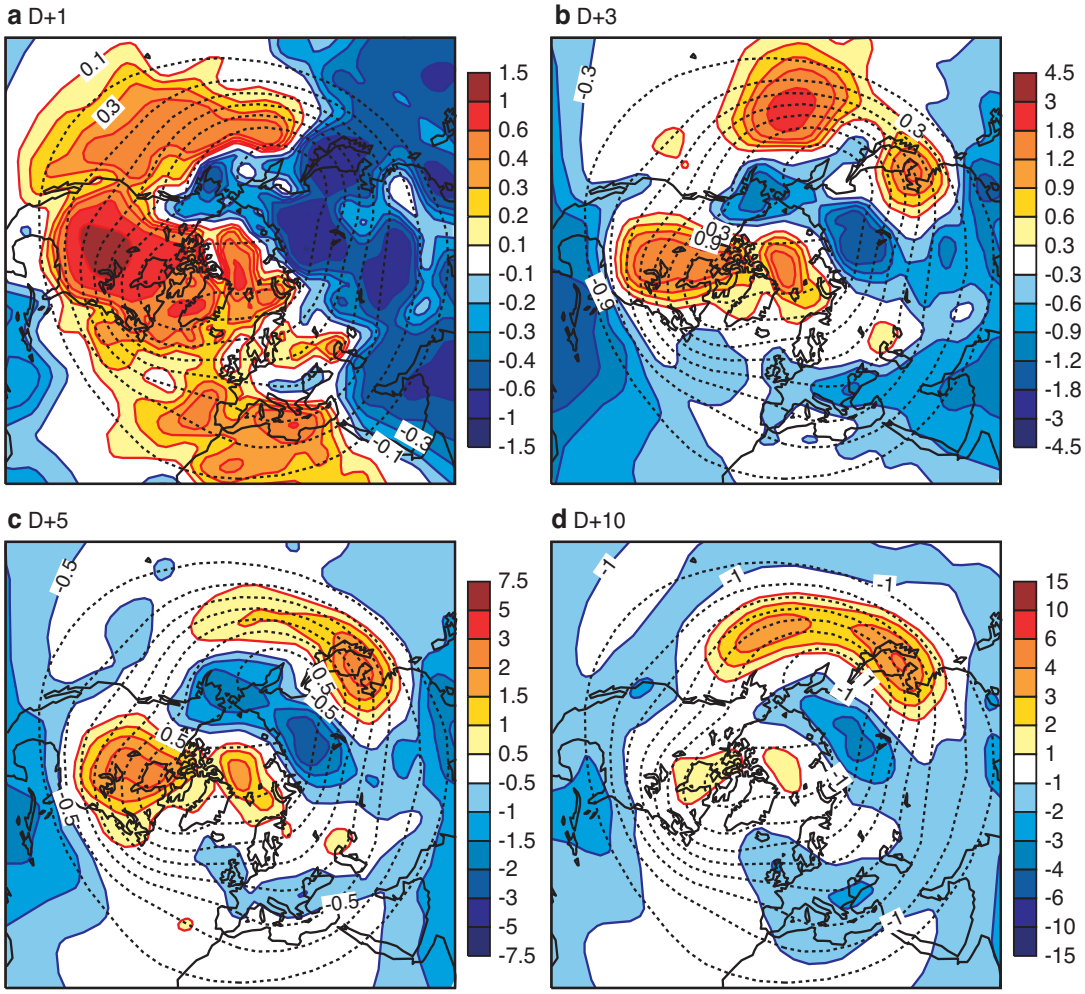

Figure 2 Systematic Z500 errors (shading in dam) of (a) D+1, (b) D+3, (c) D+5, and (d) D+10 forecasts based on model cycle 23r4 for the winters (DJFM) of 1960–2001. ERA-40 data has been used as the truth. Notice that the contour scaling changes linearly with forecast time. Also shown are the mean Z500 fields obtained from ERA-40 data (dotted contours).

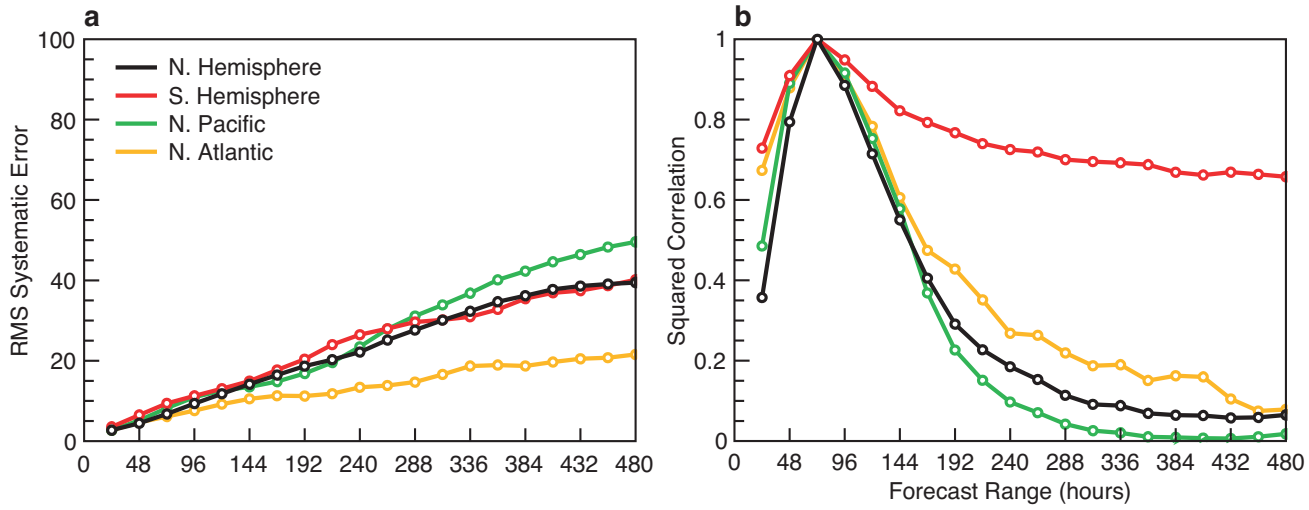

Figure 3 (a) Standard deviation (m) of systematic Z500 errors for the winters (DJFM) 2000-2003 and the Northern Hemisphere (black), Southern Hemisphere (red), North Pacific (green), and North Atlantic (yellow). (b) Squared correlation coefficients for systematic Z500 errors at D+3 with those at all other forecast steps (D+1 to D+20). Results are based on 20-day EPS control forecasts.

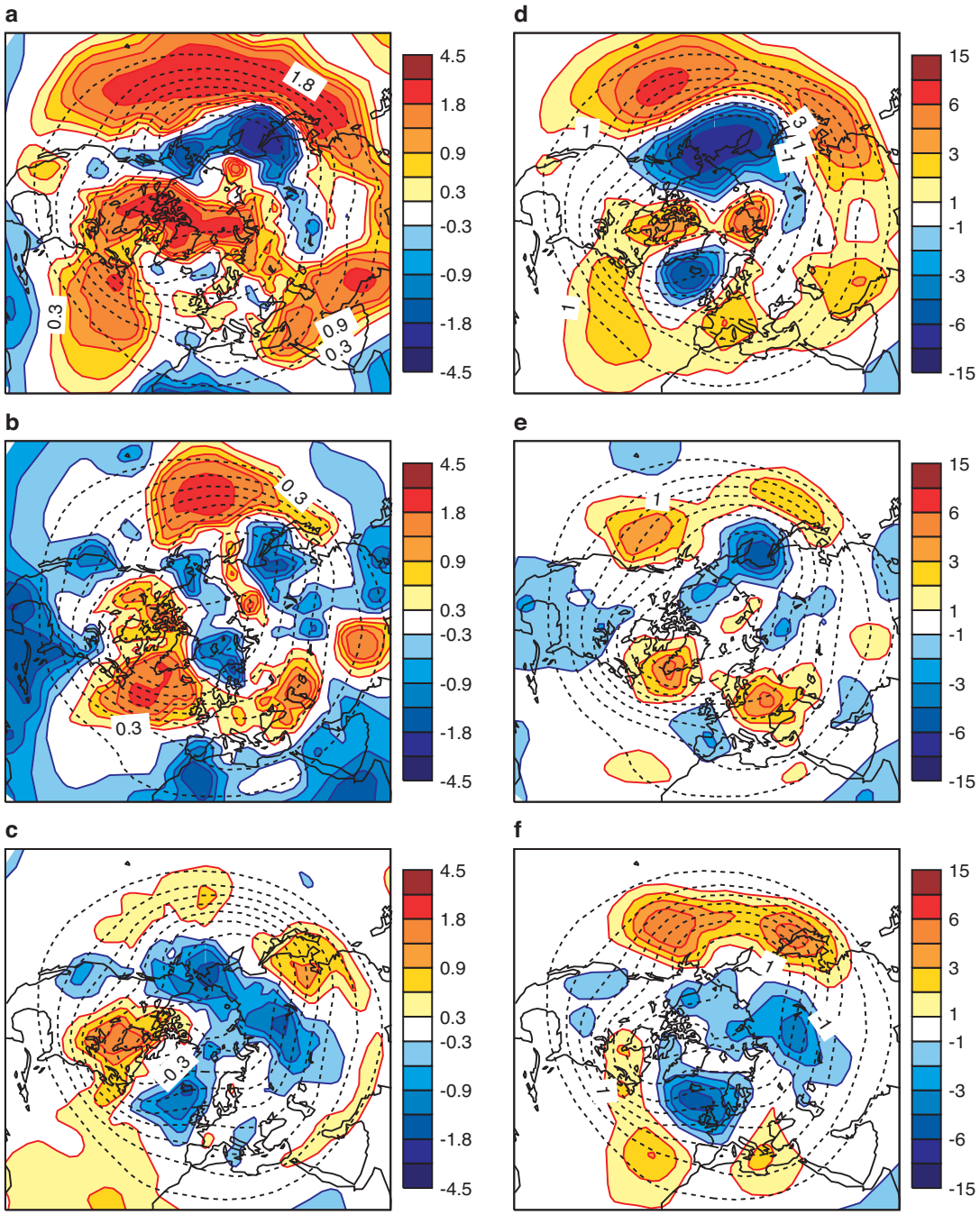

Figure 4 As Figure 2, but for the then-operational D+3 (left column) and D+10 (right column) forecasts for the period 1986-1988 (upper row), 1993–1995 (middle row), and 2001–2003 (lower row). Operational analyses were used as the truth.

Here, the removal of the systematic Z500 errors has been carried out using an empirical scheme. First, systematic Z500 errors were computed for each forecast step and grid point from the ten-day ERA-40 forecasts (winters of 1960–2001). Then, for each day, the systematic errors were removed. Finally, the Northern Hemisphere root-mean-square errors (RMSEs) were computed for the original and 'corrected' datasets. The results are shown in Figure 6(a). Evidently, the RMSEs are virtually the same for biased and 'unbiased' Z500 forecasts. At D+1 the improvement by empirically removing the bias amounts to 3%; at D+10 the improvement is less than 1% (Figure 6(b)). The results suggest that empirically removing systematic Z500 errors leads to rather minor improvements of daily Z500 forecasts, at least for geopotential height fields on a hemispheric scale. This conclusion should be interpreted carefully, however. First, weather forecasts are carried out with nonlinear models; and second, by curing model deficits that give rise to systematic errors, sources of model-related non-systematic errors might be reduced as well. In order to put the asymptotic North Pacific bias (Figure 1) into context it is worth mentioning that North Pacific Z500 anomalies during La Niña years have the

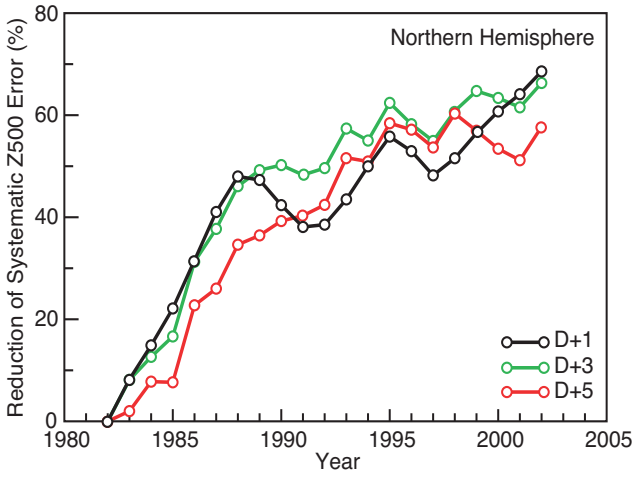

Figure 5 Reduction of wintertime Northern Hemisphere systematic Z500 errors compared with those present during the period 1981–1983 (%) at D+1 (black), D+3 (green), and D+5 (red). Each value refers to a period of three consecutive years, the centres, which are given on the time axis.

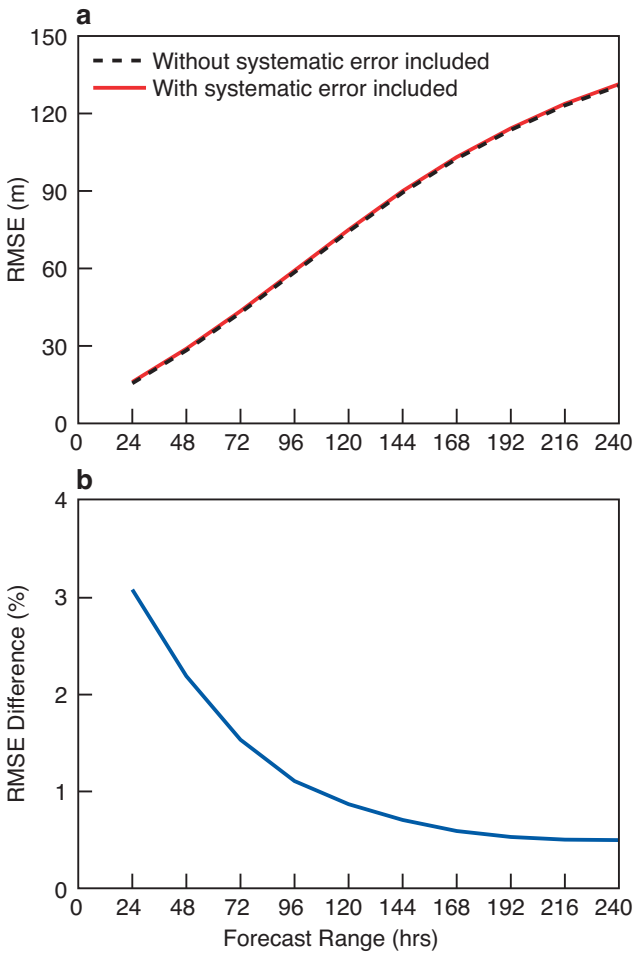

Figure 6 (a) The average root-mean-square error (RMSE) of daily Northern Hemisphere Z500 forecasts with (red) and without (black, dashed) systematic error included. (b) The difference (%) between RMSE of biased and 'unbiased' Z500 forecasts. Results are based on winters of the period 1960–2001 (cycle 23r4).

same structure and magnitude (*Hoerling et al.* 1997) as systematic errors in seasonal integrations of the ECMWF model . In the context of seasonal forecasting at ECMWF, therefore, the North Pacific bias clearly matters.

Synoptic activity

One of the goals of the Centre's research and operational activities in 1999–2008 is "… the provision of good forecasts of severe weather towards day 4 or day 5 ahead". A necessary requirement to achieve this goal is that the basic characteristics of synoptic systems are simulated well, particularly in the extratropics. In this section, possible systematic errors of the ECMWF model in simulating synoptic activity are explored.

Asymptotic systematic errors for winters of the period 1962–2001 are shown in Figure 7 for seasonal integrations based on model cycle 26r1. Here, the synoptic activity is obtained by first high-pass filtering the daily Z500 time series and then taking the standard deviation of the filtered series. The high-pass filter is such that it retains variability from two to ten days (the synoptic-frequency band). The most obvious systematic errors are found over high latitudes and the Arctic, where the model tends to underestimate observed values by as much as 25%. In mid-latitudes the performance is generally better. However, the North Pacific (North Atlantic) storm track is slightly shifted towards the north (south). Over Europe the level of synoptic activity in the model and the observations are comparable.

In the medium range, the spatial structure of systematic synoptic-activity errors is very similar to its asymptotic counterpart; the magnitude of the systematic error, however, is much lower (not shown). Further diagnosis has also revealed that most of the model improvements with respect to systematic errors took place from the 1980s to the 1990s, a finding that is in line with the results for Z500 (see Figure 4).

Euro-Atlantic blocking

The fact that winters in Western Europe are relatively mild compared with other places at the same latitude can be attributed to the existence of the Atlantic Ocean with its large heat capacity, along with the prevalence of south-westerly winds associated with the existence of the Icelandic low-pressure system. Occasionally (at about 15–20% of the days, see below) the zonal flow towards Europe is interrupted or blocked by relatively persistent anticyclones. These blocking anticyclones are associated with easterly flow, anomalously dry conditions and below-normal temperatures over wide parts of Europe. Here we show how well the ECMWF model simulates the observed characteristics of Euro-Atlantic blocking.

The observed frequency of occurrence of 'blocking days' as inferred from ERA-40 data is shown in Figure 8 for winters (December–March) of the period 1962–2001. Also shown is blocking frequency as simulated by one of the latest versions of the ECMWF model (cycle 26r1, dashed). The forecasts were started on 1 October of each year, that is, the systematic model errors had more than two months to develop. The blocking frequency has been obtained by applying the scheme of *Tibaldi and Molteni* (1990) to daily Z500: On a particular day, a given longitude is defined as being blocked if the mid-

latitude geostrophic zonal wind has an easterly component. Two maxima of atmospheric blocking are evident, one in the Euro-Atlantic area and the other over the North Pacific. After more than two months into the integration, the model clearly underestimates the blocking frequency in both regions.

Blocking tends to persist for a number of consecutive days. These spells are called blocking episodes. Here Euro-Atlantic blocking episodes are defined numerically following *Tibaldi and Molteni* (1990): A blocking episode occurs if at least three neighbouring longitude grid points (spanning 12°) are instantaneously blocked for at least four consecutive days. This condition has been slightly relaxed by allowing blocking episodes to be 'interrupted' by single days with less than three neighbouring longitudes being blocked.

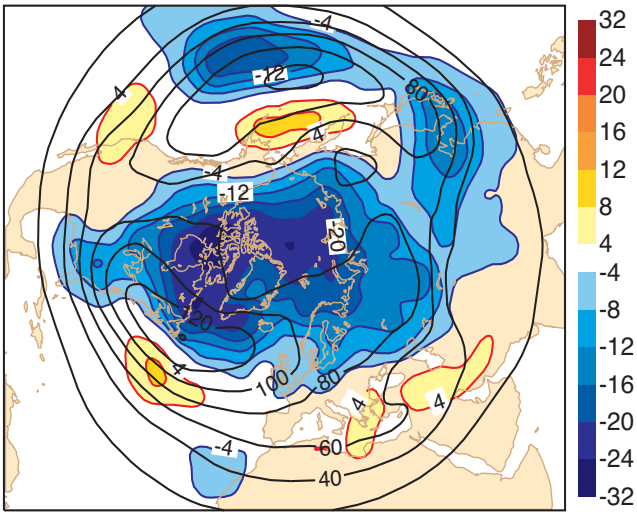

Figure 7 Asymptotic systematic error of the Z500 synoptic activity (shading in m/day) for seasonal integrations based on model cycle 26r1 (DJFM of 1962–2001). Also shown are the observed values (contours, in m/day) based on ERA-40 data. Synoptic activity has been determined by taking the standard deviation of day-to-day Z500 changes.

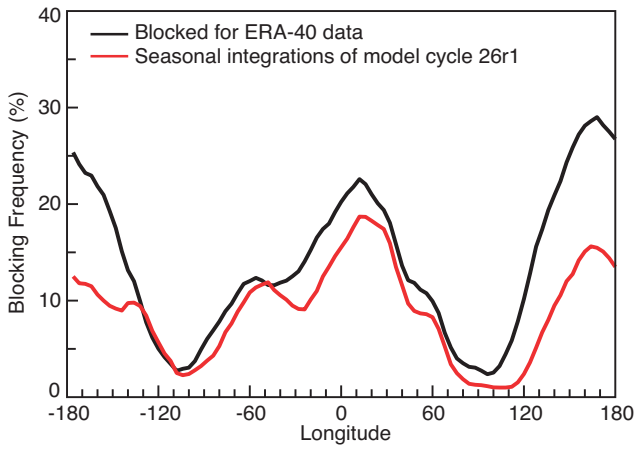

Figure 8 Frequency (%) of wintertime days (Dec–Mar) that were classified as being blocked for ERA-40 data (black) and seasonal integrations of model cycle 26r1 (red). The results are based on the period 1962-2001.

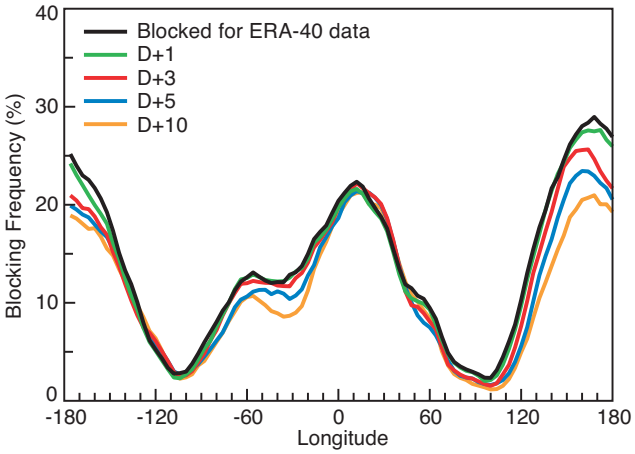

Figure 9 Frequency (%) of wintertime days (Dec–Mar) that were classified as being blocked for ERA-40 data (black) as well as D+1 (green), D+3 (red), D+5 (blue), and D+10 (yellow) forecasts based on model cycle 23r4 and the period 1960-2001.

From the ERA-40 data a total of 205 blocking episodes were found during the winters 1962–2001 (Table 2); for the same period the model simulates 188 blocking episodes, that is, the number of episodes is underestimated by about 10%. Moreover, after more than two months into the integration the model tends to overestimate (underestimate) slightly the frequency of short (long) episodes. Summarizing, systematic errors associated with Euro-Atlantic blocking amount to no more than 10% of the observed values for seasonal forecasts based on model cycle 26r1.

How large are systematic blocking errors in the short-range and medium-range forecasts? The observed frequency of occurrence of blocking for winters of the period 1960-2001 is shown in Figure 9 together with those for D+1, D+3, D+5, and D+10 forecasts. The largest systematic error in the medium range is found over the North Pacific; the frequency of occurrence over the Atlantic is slightly underestimated; and over Europe no systematic blocking errors are found in the medium range. The excellent medium-range performance of a recent version of the ECMWF model over Europe is a noteworthy achievement, given that the simulation of blocking used to be one of the key problems for earlier ECMWF model cycles (*Tibaldi and Molteni* 1990) and other atmospheric circulation models (*D'Andrea et al.* 1998). One of the key challenges in the near future regarding atmospheric blocking will be to further reduce systematic errors in extended-range forecasts, particularly in the North Pacific region.

Tropical intraseasonal variability

By far the most dominant mode of atmospheric intraseasonal variability in the tropics is associated with continental-scale organization of convection propagating eastward across the Indian and western Pacific ocean. Honouring the discoverers of this phenomenon (*Madden and Julian* 1972), this mode is nowadays known as the Madden-Julian oscillation (MJO). Regarding operational activities at ECMWF, there are at least three reasons why the MJO needs to be simulated well. First, there is evidence that westerly wind bursts can trigger

	n_{epi}	Percentage of blocking-episodes of length					
		4–6 days	7–10 days	11–15 days	16–20 days	21–30 days	>30 days
ERA-40	205	37.3	23.7	19.2	9.6	7.9	2.3
Model	188	34.9	31.4	15.7	9.9	7.6	0.6

Table 2 Total number of wintertime (Dec–Mar) Euro-Atlantic blocking episodes (n_{epi}) during the period 1962–2001 for ERA-40 data and the ECMWF model (cycle 26r1) together with the percentage of blocking-episode length (in percentage of the total number of blocking episodes) for six different length classes (4–6, 7–10, 11–15, 16–20, 21–30 and longer than 30 days). Results are based on seasonal forecasts each started on 1 October of the respective year.

ENSO events. Therefore, the skill of seasonal ENSO forecasts carried out at ECMWF may crucially depend on the model's ability to simulate the MJO. Second, there is an indication that medium-range forecast skill in the Northern Hemisphere extratropics depends on how well the tropics in general, and the MJO in particular, are simulated. Finally, the quasi-periodicity of the MJO at periods of 30–60 days implies extended-range predictability that might be utilized in monthly forecasting (see article on page 3).

The MJO has been diagnosed in a set of seasonal and medium-range forecasts. The results can be summarized as follows (*Jung and Tompkins* 2003; *Tompkins and Jung* 2004): The variance of the MJO decreases by a factor of two during the first 20 days of the integration, the model does not produce the observed spectral peak in the 30–60 day range, and the observed coherence of slowly (40–60 days) eastward-propagating anomalies is underestimated by the model; fast (20–30 days) propagating anomalies, however, are well simulated. Finally, it is found that in the ECMWF model MJO-related upper-tropospheric divergence anomalies are primarily associated with large-scale precipitation (i.e. convection on the grid-scale) instead of subgrid-scale convective precipitation (*Tompkins and Jung* 2004). Additional sensitivity experiments revealed that the periodicity of the simulated MJO depends on the ratio between large-scale to convective precipitation; the more large-scale precipitation is associated with the MJO, the more periodic the simulated MJO is. It is hypothesized that the large-scale cloud scheme constrained to provide latent heating in phase with the wave, in fact amplified a Kelvin wave. This would agree with the excessively high propagation speeds compared with the observed MJO phenomenon.

Most of the model's deficits in simulating the MJO described above are typical features of earlier model cycles and other atmospheric models as well (*Slingo et al.* 1996). Given the importance of the MJO for medium-range and extended-range forecasting improving the model's capability of properly simulating the MJO has a high priority in the near future. Possible model improvements, however, are likely to require a better understanding of the mechanisms governing the MJO. (A widely accepted theory for the MJO is still missing!)

Clouds and cloud-related parameters

In recent years much effort at ECMWF has been put into the improvement of physical aspects of the model. However, in general it is not straightforward to relate improvements in the representation of physical processes (so-called parametrizations) to parameters such as geopotential height. Therefore, and because of their paramount importance in influencing local weather conditions, a detailed study of systematic model errors should encompass clouds and cloud-related parameters. In the following, key problems of the ECMWF model in simulating cloud are summarized, followed by a comparison between the recent model cycles 26r1 and 23r4. This intercomparison aims to clarify whether model improvements during the last two years are manifest in reduced systematic cloud errors.

Previous assessment of clouds in model cycles used in the late 1990s has revealed that, in general, clouds are well captured, with the following exceptions:

- The cloud cover is too low in mid-latitudes and subsidence regions
- Too little cloud cover is simulated over Europe in summer
- The ice amount is too low, especially in the mid-latitudes
- The liquid water is too high, especially in the subtropics
- The cloud cover in stratocumulus regions is too low
- There is too much high cloud associated with tropical deep convection.

Some of the model deficits mentioned above can be inferred from Figure 10 (left column) showing the top-of-the-atmosphere short-wave radiation (TOA–SW) for model cycle 23r4 and for estimates given by the Earth Radiation Budget Experiment (ERBE), along with their difference. Results are for the summer (JJA) of 1987. Evidently, the reflectivity is too high in the subtropics and in the tropical Pacific and Atlantic. In contrast, too little cloud cover over Europe and in the stratocumulus regions off the Americas and Africa is associated with too little reflectivity. In model cycle 26r1 (Figure 10, right column) the observed TOA-SW characteristics are substantially improved in the tropical and subtropical oceans.

The improvement of cloud liquid-water paths in model cycle 26r1 compared with cycle 23r4 in the subtropics can be inferred from Figure 11, which shows model estimates together with those obtained from SSM/I retrievals.

A summary of the changes to the model physics (convection, radiation, clouds and radiation) from cycle 23r4 to 26r1, which gave rise to the above-mentioned improvements, is given in the paper by *Jung and Tompkins* (2004).

Bias improvement at Cycle 26r3

From 7 October 2003 to 8 March 2004 model cycle 26r3 was operational (Table 1). One of the major differences between cycle 26r1 and 26r3 is the aerosol climatology used. In the following we briefly discuss some preliminary results obtained from low-resolution seasonal integrations with model cycle 26r3. The focus is on precipitation, low-level wind and Z500. A more detailed survey will be given in a future publication.

Figure 12(a) shows the 'observed' mean JJA precipitation from the study by *Xie and Arkin* (1997), and the mean JJA 925hPa winds (V925) and Z500 from ERA-40. The precipitation clearly depicts the Asian summer monsoon, the

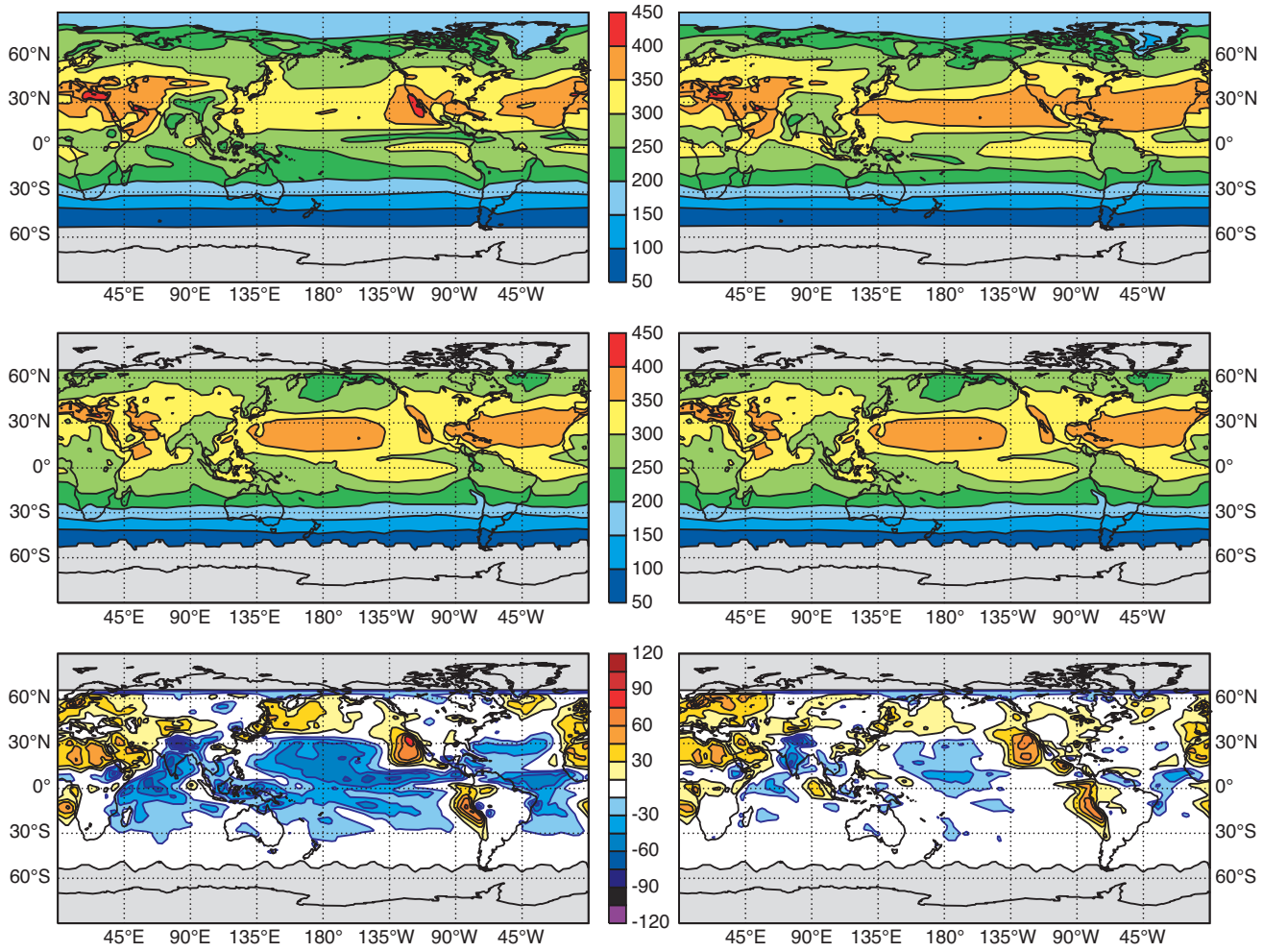

Figure 10 Mean top-of-the-atmosphere short-wave radiation (Wm^{-2}) for the period June-August 1987 based on model data (upper panels), observational data from ERBE (middle panels) along with differences between model and observational data (lower panels). Model cycle 23r4 (left) and model cycle 26r1 (right). In the upper two panels positive values are directed into the atmosphere. Positive (negative) differences indicate too little (strong) reflectivity. High latitude areas shaded in grey indicate missing data.

inter-tropical convergence zone (ITCZ) and the South Pacific convergence zone (SPCZ). The summer hemisphere Z500 field shows stronger meridional gradients over the north-western Pacific and Atlantic Oceans and, importantly, also over the Mediterranean. The monsoon cross-equatorial flow off the east coast of Africa and the oceanic-region subtropical anticyclones are visible in the low-level wind field.

Figure 12(b) shows long-term systematic differences between the observed fields and those from 40 years (1962–2001) of seasonal integrations of the low-resolution ECMWF model version 26r1. Only statistically significant differences at the 10% level are plotted. Relatively large systematic precipitation errors are seen in the Asian and North African monsoon regions with both monsoons extending too far inland but being deficient over the coastal regions. There are also major low-level wind biases over the tropical and subtropical North Atlantic, northern Africa, Saudi Arabia and Iran and elsewhere. The Z500 height bias shows the long-standing North Pacific high bias and an equally strong bias over North America. It is shown below that much of the biases in these three fields are related.

Figure 12(c) shows a similar plot for the difference between model cycle 26r3 and 26r1 and Figure 12(d) shows the difference between 26r3 and the observations. It can be seen that many of the biases at 26r1 are reduced by the transition to 26r3. In particular, the North African monsoon bias, the tropical and subtropical North Atlantic low-level wind bias and the North Pacific and North American Z500 bias are all greatly reduced at 26r3.

The reasons for this substantial improvement have been traced to the change in the aerosol climatology used in the model. At 26r1 the aerosol climatology of *Tanre et al.* (1984) was used. In this climatology, desert aerosol, particularly over the Sahara, dominates the total optical depth with peak values of 1.90 over the Sahara contributing to a total optical depth of 2.12. For 26r3, the *Tegen et al.* (1997) aerosol climatology was used (which varies with the annual cycle). This latter dataset has values of total optical depth of less than 0.4 over the Sahara. This change in aerosol climatology dramatically reduces the atmospheric short-wave absorption over the Sahara in JJA by up to 40 Wm^{-2}. Some of this implied atmospheric cooling is balanced, in the column

mean, by changes in surface long-wave and sensible heat fluxes, but there still remains a net cooling of the Saharan atmosphere of around 20 Wm^{-2}. Since this cooling maximizes in the aerosol-rich boundary layer, it acts to stabilize the atmospheric column. Hence, it cannot be balanced by convective heating and must be balanced, in the mean, by adiabatic warming due to descent. The result appears to be a reduction in instability, which inhibits the North African monsoon extending too far north.

The impact of the aerosol change is not limited to North Africa alone. The North African precipitation reduction is seen to force 'Gill-type' equatorial westward Rossby-wave and eastward Kelvin-wave responses that are associated with the improvement in Atlantic low-level wind biases and an increase in precipitation over the Arabian Sea, India, Bay of Bengal and South China Sea (see Figure 12(c)). The eastern precipitation increase generally has a beneficial impact on biases, except near India. There are also changes in precipitation along the coast of Venezuela and over Central America that are mixed in their impact on bias.

The relatively strong meridional gradients in Z500 over the Mediterranean region in JJA (noted above) are more vividly reflected at 150 hPa in the meridional gradients of absolute vorticity. In this region there is a strong upper-level southward divergent-wind change associated with the weakening of the North African monsoon. Consequently, advection of absolute vorticity by the divergent wind is strongly modified over the Mediterranean and leads to a significant positive 'Rossby-wave source' (e.g. *Sardeshmukh and Hoskins* 1988) in this region. Hence, the aerosol change also appears to be able to influence the extratropical Northern Hemisphere via the action of (non-divergent barotropic) Rossby waves and could be responsible of the improvement in the North Pacific and North American height biases. Diagnosis of medium-range forecasts tends to confirm that the changes do emanate from the African region and that the change in the shallow convective mass-flux limiter between cycles 26r1 and 26r3 (at resolutions lower that T511) plays little or no role in the bias improvements highlighted here.

The biases that remain for 26r3 now point to convection errors in a region whose centre lies between the Philippines and Taiwan. It is clear (from equatorial wave dynamics) that an improvement in convection in this region will coincide with a major beneficial impact on the remaining global

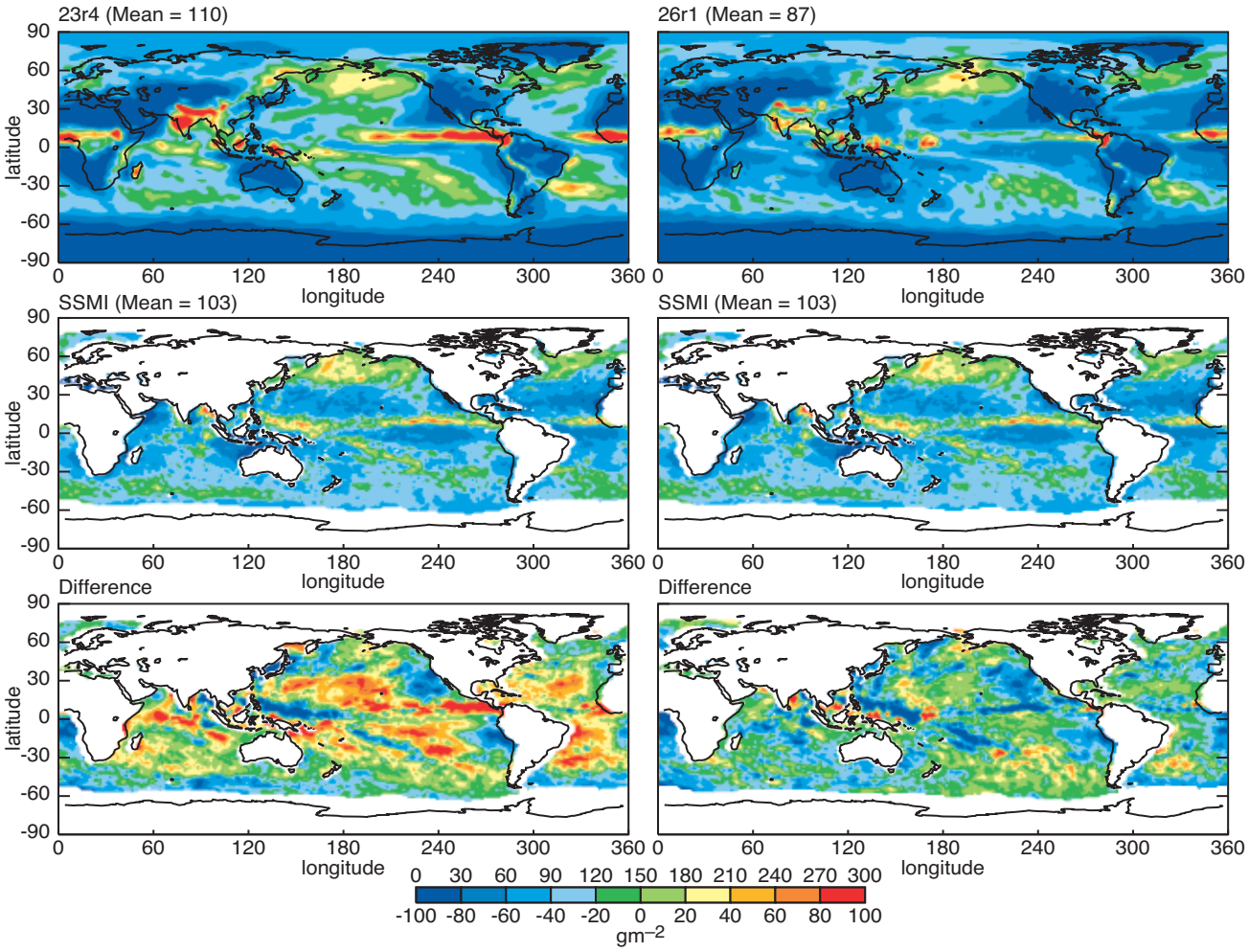

Figure 11 Mean cloud liquid-water path (gm^{-2}) for June–August 1987 based on model data (upper panels), observational estimates from SSM/I (middle panels) along with differences between model and observational data (lower panels). Model cycle 23r4 (left) and model cycle 26r1 (right). No data is available over the land.

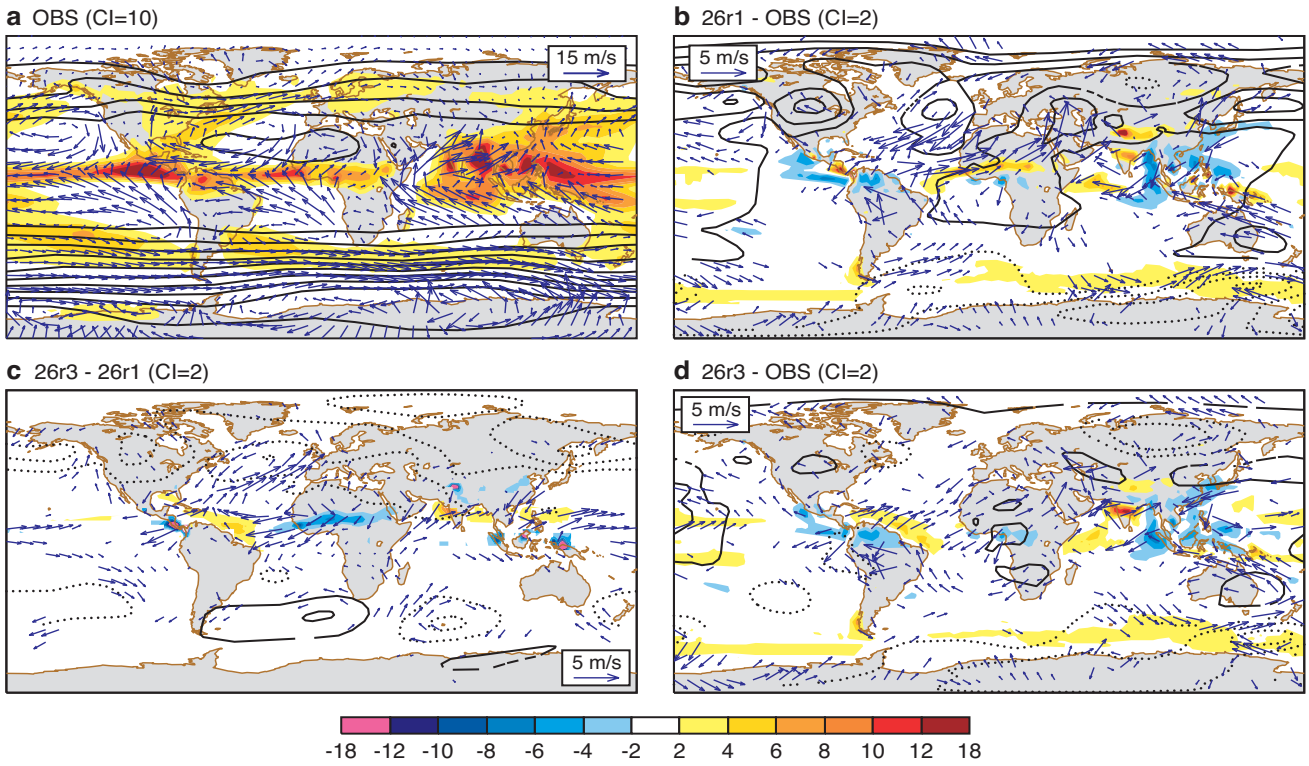

Figure 12 (a) Observed mean precipitation (shaded in mm/day), Z500 (contours), and wind vectors at 925hPa (V925, vectors) for JJA. (b) Systematic errors for precipitation, Z500 and V925 for model cycle 26r1. (c) As (b), but for the difference between 26r3 and 26r1. (d) As (b), but for model cycle 26r3. In (b)–(d) only statistically significant differences (at the 10% level) are shown for Z500 and V850. The contour intervals for Z500 are given by Ci in the titles. Observational precipitation data are taken from *Xie and Arkin* (1997) for the period 1980–99. Simulated values of Z500 and V925 are verified against ERA-40 data (1962–2001).

circulation biases. The influence of the Asian "brown cloud" aerosol is currently being investigated. The deterioration in Indian precipitation bias for 26r3 may be related to a strong and small-scale maximum in total aerosol optical depth over the Horn of Africa and Arabian Sea in the new aerosol climatology. The atmospheric heating associated with this aerosol is not likely to be offset by any compensating surface heat fluxes over the Arabian Sea (which has a larger effective heat capacity than the African landmass) and could be enough to allow the monsoon inflow to break through the boundary-layer inversion, thus setting-off convection. This possibility is currently being investigated.

The winter season has also been briefly examined. The model changes introduced in model cycle 26r3 also appear to have a beneficial impact on the atmospheric circulation. The North Pacific Z500 bias (see Figure 1), for example, shows major improvements at 26r3 compared to earlier model cycles.

Further reading

Articles on atmospheric circulation and phenomena

Hoerling, M.P., A. Kumar & **M. Zhong**, 1997: El Nino, La Nina and the nonlinearity of their teleconnections. *J. Climate*, **10**, 1769-1786

Madden, R.A. & **P.R. Julian**, 1972: Description of global-scale circulation cells in the tropics with a 40-50 day period. *J. Atmos. Sci.*, **29**, 1109-1123

Sardeshmukh, P.D. & **B.J. Hoskins**, 1988: The generation of global rotational flow by steady idealized tropical divergence. *J. Atmos. Sci.*, **45**, 1228-1251

Xie, P. & **P.A. Arkin**, 1997: Global precipitation: A 17-year monthly analysis based on gauge observations, satellite estimates and numerical-model outputs. *Bull. Amer. Meteorol. Soc.*, **78**, 2539-2558

Articles on modelling and model systematic errors

Andersson, E., A. Beljaars, J. Bidlot, M. Miller, A. Simmons & **J-N. Thépaut**, 2003: A major new cycle of the IFS: Cycle 25r4. *ECMWF Newsletter*, **97**, Spring 2003, 12-20

D'Andrea, F. & co-authors, 1998: Northern Hemisphere atmospheric blocking as simulated by 15 atmospheric general circulation models in the period 1979-1988. *Climate Dyn.*, **14**, 385-407

Ferranti, L., T.N. Palmer, F. Molteni & **E. Klinker**, 1990: Tropical-extratropical interaction associated with the 30–60 day oscillation and its impact on medium and extended-range prediction. *J. Atmos. Sci.*, **47**, 2177-2199

Jung, **T**. & **A.M. Tompkins**, 2003: Systematic errors in the ECMWF forecasting system. *ECMWF Technical Memorandum,* **422**, http://www.ecmwf.int/publications/library/do/references/list/14

Slingo, **J.M.** & co-authors, 1996: Intraseasonal oscillations in 15 atmospheric general circulation models: Results from an AMIP diagnostic subproject. *Climate Dyn.*, **12**, 325-357

Tanre, **D.**, **J-F. Geleyn**, and **J.M. Slingo**, 1984: First results of the introduction of an advanced aerosol-radiation interaction in the ECMWF low-resolution global model. Pp. 133-177 in Aerosols and their climate effects. Editors H. E. Gerber and A. Deepak. A. *Deepak Publications*, Hampton, Va., USA

Tegen, **I.**, **P. Hollrig**, **M. Chin**, **I. Fung**, **D. Jacob**, and **J. Penner**, 1997: Contribution of different aerosol specifies to the global aerosol extinction optical thickness: Estimates from model results. *J. Geophys. Res.*, **102**, 23895-23915

Tibaldi, **S.** and **F. Molteni**, 1990: On the operational predictability of blocking. *Tellus*, **42A**, 343-365

Tompkins, **A.M.** and **T. Jung**, 2004: 'Influence of process interactions on MJO-like convective structures in the IFS model'. Pp 103–114 in *ECMWF workshop proceedings* on simulation and prediction of intra-seasonal variability.

Thomas Jung, Adrian Tompkins, and Mark Rodwell

Towards freak-wave prediction over the global oceans

Presently, there are at least two classes of extreme wave events known to us that may occur at sea. The first type of event typically has a large scale, of the order of 100 km, and can be classified as a shallow-water event. I will call these extreme events 'tsunamis'. They are generated by, for example, earthquakes or volcanic activity at the bottom of the ocean or by landslides. Because of the nature of the cause, these extreme events occur very infrequently and are difficult to predict. If generated by earthquakes, tsunamis are usually just a small amplitude disturbance in the mean sea level of the order of a few centimetres, but the scale of the disturbance is large. When a Tsunami reaches coastal areas and the depth of the ocean decreases, the front of the disturbance slows down and, by conservation of mass, the local amplitude of the disturbance starts to increase. The end result is a massive wall of water propagating towards the shore resulting in large damage and many casualties (*Dudley and Lee* 1998). In the North Pacific there is a warning system in place that is capable of detecting small systematic deviations from the mean sea level. If detected on time, people in the relevant coastal areas may be evacuated. However, the propagation speed of such a large-scale phenomenon may reach speeds of the order of 700 km/hr, and therefore, when such an event is generated near coastal areas, warning and evacuation may not be possible.

The second type of extreme event is of a small scale, at most 1 km and, as it usually occurs in the open ocean, it can be classified as a deep-water phenomenon. These extreme ocean waves are wind waves and are called Freak Waves or Rogue Waves. The first evidence on Freak Waves was anecdotal and came from sailors. However, the proof of their existence was cast in doubt by many scientists until, in the last decade, firm evidence was provided from observations based on laser measurements.

In this article I will first describe what is meant by a freak-wave event, which indicates an abnormal sea state. Next, the present state of the art of understanding the causes for the generation of freak waves is given. This is followed by a discussion of how to predict the probability of extreme events such as freak waves in the context of operational wave forecasting. Finally, from the present understanding of freak waves it will follow immediately why, at sea, it is so difficult to verify forecasting results for freak waves. However, in the laboratory there is more control of the circumstances, and the theory of freak-wave prediction has recently been validated successfully.

Linear waves

As freak waves are associated with an abnormal sea state, it is important to define what is meant by normal conditions. Most of the time ocean waves have small amplitudes and may be described by linear theory. In the linear approximation, waves do not interact with each other so that the superposition principle holds. Imagine that, at a certain location somewhere in the middle of the ocean, one observes the ocean waves propagating from far-away well-separated regions of the oceans. For all practical purposes, these linear ocean waves may be regarded as independent. Even when they come from the same direction, if they have travelled a sufficiently long distance the waves will have dispersed. Therefore, in the region of interest, waves from the same source area must have been generated at different times and are therefore independent. Consequently, by the central-limit theorem, the distribution of the surface elevation is Gaussian. This so-called normal distribution is the norm, and it is observed most of the time on the open ocean. The Gaussian is determined by one parameter, namely the width σ of the distribution. For linear ocean waves, the width σ is related to the significant-wave height H_S by the relation $H_S = 4\sigma$; hence the significant-wave height is one of the key parameters predicted by ocean-wave forecasting systems.

In the framework of linear theory, it is now straightforward to estimate the probability of extreme events. According to the normal distribution, an extreme event (defined as one where the surface elevation is twice the significant-wave height) occurs every 15,000 waves. With a typical wave period of 10 s, this implies that an extreme event occurs every 40 hours, which is much longer than the typical timescale of wind variability. Note that this definition of an extreme event is a relative one because extreme-wave events are related to the average sea state. Hence, an event with a wave height of 2.5 m is regarded as extreme if the average sea state is 1.25 m or less. Although such an event is a trivial matter for an oil tanker, a small sailing boat might end up in serious trouble.

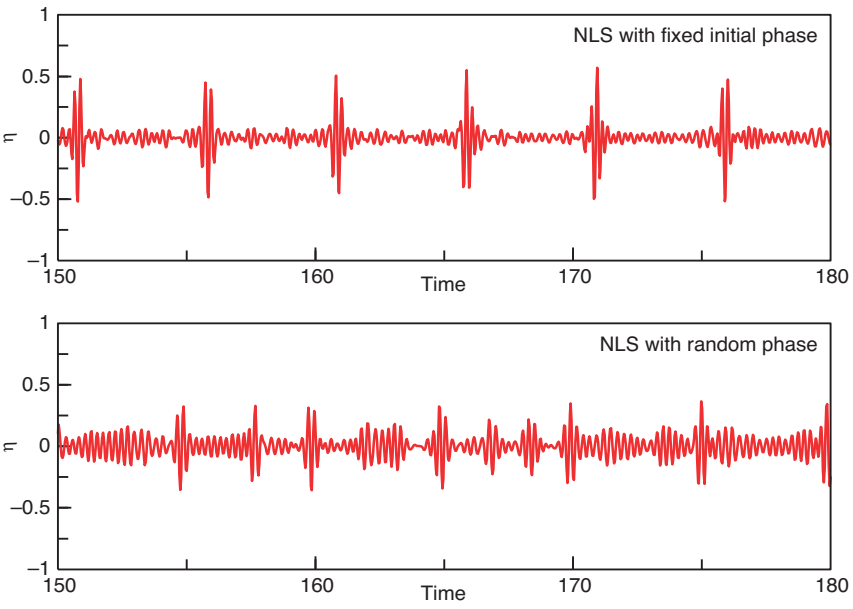

Figure 1 Dependence of the formation of freak waves on the initial choice of the phase of the waves. Top panel: constant phase; bottom panel: random phase.

nonlinear waves and focusing

In linear theory the main mechanism for the generation of extreme events turns out to be constructive interference. Consider a surface-elevation signal consisting of two waves with the same amplitude and nearly the same wavelength. Then, in linear theory, if the phases of the two waves are chosen appropriately, interference may give, at best, a surface elevation of twice the amplitude. Hence, by choosing the phases in a proper manner, there is constructive interference. For other choices of the phase of the waves there is only destructive interference. From this point of view, it is clear that the occurrence of extreme events depends on the initial choice of the phases of the waves. However, at sea the phases of the waves are not known, and therefore one has to resort to a statistical approach. For many waves with random phase this gives, in linear theory, the already-mentioned normal distribution for the surface elevation.

It is important to realise that finite-amplitude effects (also called effects of nonlinearity) may change this picture quite dramatically. Ocean waves are the solution of a nonlinear set of partial differential equations. For a typical steepness (defined as the product of the wave number $2\pi/\lambda$ (λ being the wave length) and the amplitude a of the wave) of 0.1, the phase speed of the nonlinear wave is only 0.5% larger than the corresponding linear phase speed. Nevertheless, over large timescales, of the order of 10–100 wave periods, nonlinearity may give rise to considerable changes in the surface elevation. The new element introduced by nonlinearity is that ocean waves are allowed to interact with each other, but the interaction takes only place when a certain number of selection rules are obeyed. For deep-water gravity waves these selection rules imply that this interaction is efficient when at least four waves are involved (four-wave interactions). As a consequence, nonlinear focusing results, which may counteract the linear dispersion of waves. The result of this balance between nonlinearity and dispersion is that stable wave groups are formed which may last for a long time[1].

The idea of nonlinear focusing was confirmed by an important laboratory experiment performed by Benjamin and Feir. At one end of a wave tank they generated an almost uniform wave-train, i.e. a wave-train consisting of a single frequency and almost constant amplitude (hence, the envelope was almost constant). Further down the wave tank they observed that the wave-train changed to a deeply modulated state, indicating the formation of nonlinear wave groups. This important experimental and theoretical result triggered a lot of interest in the nonlinear dynamics of waves, resulting in two main results. The first one was that the nonlinear evolution of a wave group could be well described by an approximate evolution equation, called the nonlinear Schrödinger equation (NLS)[2]. Secondly, it could be solved exactly. The main ingredient of its solution was the formation of stable wave groups (called envelope solitons).

An important consequence of the exact theory for freak-wave generation was recently discovered by *Onorato et al.* (2000). They found that, owing to nonlinear focusing, constructive interference would give rise to a three-fold increase in amplitude of the surface elevation rather than the factor of two found in linear theory. For two-dimensional propagation even larger amplification factors are found. Hence, as expected for extreme events, nonlinearity plays an important role in the formation of freak waves.

As an illustration of the importance of the combination of nonlinearity and of the initial choice of the phases of the waves, I show in Figure 1 two time series of the surface elevation (multiplied by the wave number) obtained from a numerical integration of the NLS equation. Both start from the same energy distribution (hence amplitude) as function of wave number but, in the top panel, all phases are equal

1 In nonlinear optics one attempts to make use of this property of stable nonlinear wave groups to have a robust method of information transfer.

2 Note that this evolution equation has been found in many other fields as well, such as nonlinear optics and plasma physics.

initially while in the bottom panel the phases have been chosen at random. Clearly, in the top panel nonlinear wave groups, or envelope solitons, are seen which, no doubt, must give serious problems for a ship when encountering such extreme sea states.

Prediction of extreme events

From the previous discussion it is clear that freak waves can only arise when the waves are sufficiently coherent (meaning almost equal phase as function of wave number). In these circumstances, when the waves are sufficiently steep, nonlinear focusing can do its work giving extreme sea states. These favourable conditions for freak-wave formation can be measured by means of a dimensionless parameter called the Benjamin-Feir Index (BFI). Noting that the coherency of a wave system can be measured by means of the width of the corresponding wave spectrum, the BFI is basically the ratio of the steepness of the waves and the width of the spectrum. Large values of the BFI index (in practice of the order of 0.5) correspond to favourable conditions for freak waves to occur.

At this point, the question arises whether it will be possible to predict the occurrence of freak waves. The prediction of individual extreme states seems to be impossible, because their generation depends on the initial phases of the waves. Even if one knows the initial phases, it turns out that the prediction of the phase can only be done for a relatively short time; it is known that the nonlinear evolution of the phase becomes chaotic after just a few hundred wave periods. Therefore, one has to resort to a prediction of the statistical properties of the sea surface elevation.

Just recently, it has been shown that, when four-wave interactions are important, there is a direct correspondence between the wave spectrum (namely through the BFI) and the kurtosis of the probability distribution of the surface elevation (*Janssen* 2003). When the BFI is small, the kurtosis is about three, corresponding to its value for a normal distribution. For increased values of the BFI, the kurtosis increases rapidly to values of the order of four, suggesting a sharp increase in the probability of the occurrence of extreme events.

Following these theoretical developments, we have introduced into the ECMWF operational wave forecasting system (CY26r3) some additional wave parameters characterizing extreme events, namely the BFI and the kurtosis parameter. From the kurtosis one may obtain the enhanced probability of extreme events (*Janssen and Bidlot* 2003). As an example, in Figure 2 the one-day forecast enhancement is shown for 8 February 2004. As expected, in most locations the probability distribution of the surface elevation is close to the normal distribution, as is reflected by the enhancement being close to one. In only a few locations extreme sea states are found, for example east of Newfoundland where the enhancement is nearly a factor of five. In those circumstances one expects an extreme event every eight hours, rather than every forty hours as obtained from linear theory.

Validation issues

Regarding validation of the prediction of freak wave events there are a number of issues to be raised.

First, it should be checked whether our wave prediction system is capable of modelling a new wave parameter, such as the BFI, in a viable way. In order to check this, we compared the modelled BFI with the observed BFI obtained from observed buoy spectra. A favourable agreement was obtained (*Janssen and Bidlot* 2003).

Second, the theoretical relation between the BFI and the kurtosis of the surface elevation probability distribution needs to be checked. Recently, *Onorato et al.* (2004) performed experiments in a big wave tank (10 m wide, 10 m deep and 250 m long) in Trondheim. They used realistic initial wave spectra while the phases of the waves were random, so that

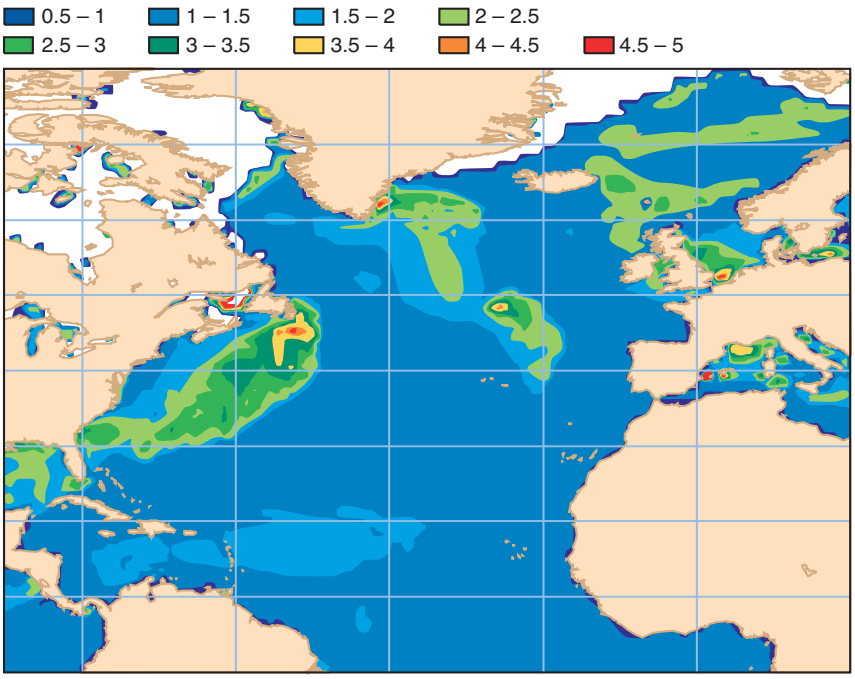

Figure 2 One day forecast of enhanced probability of extreme events for the 8th of February 2004

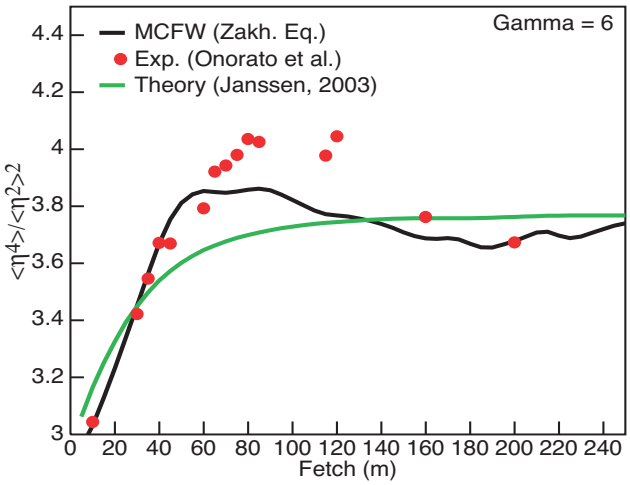

Figure 3 Kurtosis $<\eta^4>/<\eta^2>^2$ as a function of the fetch. Shown is a comparison between Monte Carlo forecasting of waves (MCFW), theory and experimental results by *Onorato et al.* (2004).

at the beginning of the wave tank the waves obeyed a normal distribution with kurtosis values close to three. As illustrated in Figure 3, they observed a rapid increase of kurtosis down the wave tank as function of 'fetch'. The fetch dependence on kurtosis was well simulated by an ensemble prediction system for waves (basically doing Monte Carlo forecasting of waves (MCFW) with the deterministic evolution equations) and by the theory for the ensemble mean.

Third, validation of actual forecasts of extreme events is at the moment an unresolved issue. For example, from the foregoing discussion it is evident that the kurtosis parameter depends on the 'unpredictable' phases of the waves, therefore only ensemble averages, temporal averages or spatial averages are meaningful quantities to verify. However, in the field we only have buoys measuring time series of about 10–20 minutes long, which corresponds to an average over between 60 and 120 waves. The small probabilities we are dealing with here (say of the order of one every 10,000 waves) can, of course, not be determined in a reliable way from such a small sample.

Clearly, we need to get confidence in our capabilities of forecasting extreme events. With all the caveats in mind it would be useful for marine forecasters to start checking the new wave parameters in case ships report extreme events. In fact, the actual case displayed in Figure 3 was plotted after Lennart Cederberg (Swedish Meteorological and Hydrological Institute) reported to the present author by phone that, in the early hours of 8 February 2004, a ship's master had observed abnormal waves (in this case breaking waves of 10 m height) on the ship's radar once every 50 minutes, or so. Indeed, according to our (extreme) wave forecasting system, an extreme sea state was expected, which is reassuring. However, it is clear that much more evidence is needed in order to build confidence in our ability to predict extreme events.

Further reading

Articles on observations of waves

Dudley, W.C. & **M. Lee**, 1998: Tsunami! 2nd edition. *University of Hawaii Press*

Onorato, M., A.R. Osborne, M. Serio, L. Cavaleri, C. Brandini & **C.T. Stansberg**, 2004: Extreme waves and modulational instability: Wave-flume experiments on irregular waves. *J. Fluid Mech.*, (in press)

Articles on wave theory

Benjamin, T.B. & **J.E. Feir**, 1967: The disintegration of wave trains on deep water. Part 1. Theory. *J. Fluid Mech.*, **27**, 417-430

Janssen, P.A.E.M., 2003: Nonlinear four-wave interactions and freak waves. *J. Phys. Oceanography.*, **33**, 863-884

Janssen, P.A.E.M. & **J. Bidlot**, 2003: New wave parameters to characterize freak wave conditions, *ECMWF Research Memo R60.9/PJ/0387*, ECMWF, Shinfield Park, Reading, RG2 9AX, UK

Onorato M., A.R. Osborne & **M. Serio**, 2000: 'nonlinear dynamics of rogue waves'. Pp. 470-479 in *Proceedings of the 6th international workshop on wave hindcasting and forecasting*, Monterey, Ca., USA, November 6–10

Peter Janssen

Member State computer resources 2004

Member State	HPCF (kunits)	Data Storage (Gigabytes)
Belgium	1447	9378
Denmark	1217	7890
Germany	6440	41743
Spain	2369	15357
France	4707	30507
Greece	1093	7087
Ireland	973	6309
Italy	3950	25598
Luxembourg	800	5188
Netherlands	1833	11883

Member State	HPCF (kunits)	Data Storage (Gigabytes)
Norway	1178	7635
Austria	1311	8501
Portugal	1055	6840
Switzerland	1520	9853
Finland	1096	7106
Sweden	1406	9117
Turkey	1303	8449
United Kingdom	4813	31196
Special Projects	3629	20363
Total	**42140**	**270000**

Special Project allocations 2004–2006

Member State		Institution	Project title	2004		2005		2006	
				HPCF units	Data storage	HPCF units	Data storage	HPCF units	Data storage
Continuation Projects									
Austria	1	Univ. Graz (Kirchengast)	Climate Monitoring by Advanced Spaceborne Sounding and Atmospheric Modelling	30000	250	30000	300	30000	300
	2	Universitat fur Bodenkultur, Vienna (Kromp-Kolb)	Modelling of Tracer Transport (MoTT)	500	5	500	5	500	5
	3	Univ. Vienna (Steinacker)	Mesoscale Alpine Climatology (VERACLIM)	100	5	100	5		
Denmark	4	DMI (Sattler, Feddersen)	Investigations on LAM ensembles for wind power prediction (WEPS)	70000	250	70000	250	70000	250
France	5	L.A.M.P. (Cautenet)	Chemistry, cloud and radiation interactions in a meteorological model	100	2	100	2	100	2
	6	Mercator-Ocean (de Prada)	MERCATOR	540000	3500	540000	3500	540000	3500
	7	MPI-A Heidelberg (Masciadri)	Forecasting of the optical turbulence for Astronomy applications with the Meso-NH mesoscale model coupled with ECMWF products	4000	30	4000	30	4000	30
	8	CERFACS (Morel)	Universal software for data assimilation	10000	180	10000	180	10000	180
	9	CERFACS (Ricci)	Variational data assimilation: background error covariance matrix	10000	150	10000	150	10000	150
	10	CERFACS (Rogel)	Seasonal to interannual predictability of a coupled ocean-atmosphere model	10000	150	10000	150	10000	150
Germany	11	MPI, Hamburg (Bengtsson)	Numerical experimentation with a coupled ocean/atmosphere model	180000	900	220000	1250	260000	1500
	12	MPI, Hamburg (Bengtsson)	Simulation and validation of the hydrological cycle	190000	900	265000	1500	350000	2200
	13	Freie Univ. Berlin (Cubasch, Kirchner)	Investigation of systematic tendency changes and their influence to the general circulation simulated with climate models	5000	800	6000	1000	8000	1500
	14	ISET (Czisch)	Evaluation of the Global Potential of Energy Towers	100	20	100	20	100	20
	15	D.L.R. (Doernbrack)	Influence of non-hydrostatic gravity waves on the stratospheric flow for field above Scandinavia	40000	80	45000	80	45000	80
	16	Univ. Munich (Egger, Gantner, Pfeiffer)	Landsurface – Atmosphere interaction	15000	100	15000	100	15000	100
	17	D.L.R. (Hoinka, Egger)	Climatology of the global tropopause	7000	10	8000	10	10000	10
	18	IMK-IFU (Kuntsmann)	On-Set of the Rainy Season in West Africa	40000	100	40000	100	40000	100

Member State		Institution	Project title	2004		2005		2006	
				HPCF units	Data storage	HPCF units	Data storage	HPCF units	Data storage
Continuation Projects									
Germany	19	MPI, Hamburg (Manzini)	Middle atmosphere modelling	180000	950	210000	1350	250000	1500
	20	Alfred Wegener Institute (Rinke)	Sensitivity of HIRHAM	200	50	1000	50	1000	50
	21	Alfred Wegener Institute (Schollhammer, Rex)	Changes in ozone transport: residual circulation and the isentropic transport	200	10	200	10	200	10
	22	MPI, Hamburg (Schultz)	Global Atmospheric Chemistry Modelling	80000	1000	80000	1500	80000	2000
	23	Univ. Koln (Speth)	Interpretation & calculation of energy budgets	100	6	100	6	100	6
	24	Univ. Munich (Stohl, James)	Validation of trajectory calculations	1000	80	1000	90	1000	100
	25	Univ. Bremen (Weber)	Chemical and dynamical influences on Decadal Ozone Change (CANDIDOZ)	100	20	100	20	100	20
	26	Univ. Mainz (Wirth)	Water vapour in the upper troposphere	1000	20	1000	20	1000	20
Ireland	27	Univ. College Cork, INM (Joergensen, Moehrlen, Garcia Moya)	HONEYMOON – A high resolution numerical wind energy model for on- and offshore forecasting using ensemble predictions	21000	10				
	28	Met Éireann (Lynch)	Community Climate Change Consortium for Irelan (C4I)	30000	1000	50000	1000	50000	1000
	29	Univ. College Cork, Met Éireann (Moehrlen, McGrath, Joergensen)	Verification of Ensemble Prediction Systems for a new market: Wind Energy	21000	20	21000	20		
Italy	30	ISMAR-CNR (Cavaleri)	Evaluation of the performance of the ECMWF meteorological model at high resolution	20000	150	20000	150	20000	150
	31	ICTP, Trieste (Molteni)	nonlinear aspects of the systematic error of the ECMWF coupled model	30000	120	30000	120	30000	120
	32	ARPA-SMR, Emilia Romagna & Italian Met. Service (Paccagnella/Montani/Ferri)	Limited area model targeted ensemble prediction system (LAM-TEPS)	80000	50	90000	60	100000	70
Netherlands	33	KNMI (Drijfhout)	Agulhas	20000	0	20000	0	20000	0
	34	KNMI (van Oldenborgh, Burgers)	Advanced ocean data assimilation	50000	100	50000	100	50000	100
	35	KNMI (Siebesma)	Large Eddy Simulation (LES) of boundary layer clouds	25000	30	25000	30	25000	30
Norway	36	DNMI (Frogner)	REGCLIM: optimal forcing perturbations for the atmosphere	150000	500	200000	500	200000	500
	37	Univ. Oslo (Isaaksen, Sundet)	Ozone as a climate gas	15000	5	15000	5	15000	5
Portugal	38	Univ. Lisbon (Soares)	HIPOCAS–SPEC	0	10	0	10	0	10

Member State		Institution	Project title	2004		2005		2006	
				HPCF units	Data storage	HPCF units	Data storage	HPCF units	Data storage
Continuation Projects									
Spain	39	Univ. Illes Balears (Cuxart)	Study of the Stably stratified Atmospheric Boundary Layer through Large-Eddy simulations and high resolution mesoscale modelling	60000	100	60000	100	60000	100
Sweden	40	SMHI (Unden)	The Hirlam 6 project	250000	1500	35000	2000	500000	2500
United Kingdom	41	ESSC, Univ. Reading (Bengtsson)	Sensitivity of ERA-40 to different observing systems and determination of the Global Water Cycle	250000	300	250000	300	300000	300
	42	Univ. Reading (Hoskins)	Routine back trajectories	5000	4	5000	4	5000	4
	43	Univ. Reading (Hoskins)	Stochastic physics	20000	90	20000	90		
	44	DARC, Univ. Reading (O'Neill)	Reanalysis for the 1990s using UARS data	300000	1000				
	45	BAS, Cambridge (Turner, Lachlan-Cope)	Assessment of ECMWF forecasts over the high latitude areas of the Southern Hemisphere	0	1	0	1	0	1
JRC	46	JRC-IES (Dentener)	The linkage of climate and air pollution: simulations with the global 2-way nested model TM5	15000	100	15000	100	150000	100
New Projects									
Austria	1	Univ. Vienna (Beck, Ahrens)	Alpine regional downscaling of reanalysis data using the LAM ALADIN	500	100	1000	100	1000	100
	2	Univ. Innsbruck (Ehrendorfer)	Mesoscale Predictability and Ensemble Prediction	8000	5	8000	5	8000	5
	3	Univ. Vienna (Haimberger)	Checking the temporal homogeneity of the ERA-40 observational input and analyses using analysis feedback data	500	200	1000	200		
Total requested				**2785400**	**14963**	**2483200**	**16573**	**3270100**	**18878**

The history of ECMWF – A call for contributions

Following suggestions of delegates to the Council last year, I am preparing to write the History of the Centre. I plan to complete the text in early 2005, with a view to publishing the history in time for the Centre's 30th anniversary on 1 November 2005. I hope also to prepare a DVD to accompany the book.

I would welcome proposals for material for inclusion. Since I am now collecting background information, I would welcome an early indication of the availability of such material.

Please email me: Austin.Woods@ecmwf.int

Austin Woods

ECMWF Workshops and Scientific Meetings 2004

Workshop on the Hydrological Ensemble Prediction Experiment (HEPEX) (8–10 March)

ECMWF hosted the International Hydrological Ensemble Prediction Experiment (HEPEX) Workshop. The workshop was organized under the auspices, and with the help of, NOAA, ECMWF, WCRP/GEWEX, IAHS/PUB and WMO/HWR.

Objectives

The main objective of HEPEX is to bring the international hydrological community together with the meteorological community to demonstrate how to produce reliable hydrological ensemble forecasts that can be used with confidence by the emergency management and water resources sectors to make decisions that have important consequences for the economy, for public health and safety.

Representatives of operational hydrological services and operational water resources agencies are expected to participate in helping to define and execute the project. The HEPEX objective can be achieved if the meteorological, hydrological and water resources communities understand the key challenges they face and work together both to couple currently available forecasts tools and to improve the current quality of available systems.

Further information

http://www.ecmwf.int/newsevents/meetings/workshops/2004/HEPEX/index.html

WISE meeting – Waves In Shallow water Environment (6-10 June)

Objectives

The WISE meeting is a yearly gathering of ocean wave modellers. It is a continuation of the successful WAM (Wave Model) group collaboration, which produced the WAM model in the 1980s. This model has been running operationally at ECMWF since 1992.

Further information can be found on the WISE website: http://www.surf-link.com/wise/

Organizers

Dr Luigi Cavaleri (ISMAR): cavaleri@ismar.cnr.it
Dr Peter Janssen (ECMWF): peter.janssen@ecmwf.int

Workshop on Assimilation of High-Spectral-Resolution Sounders in NWP (28 June–1 July)

Objectives

The NASA AQUA satellite was successfully launched in May 2002 and sampled radiance data from the AIRS (and the accompanying AMSU-A) instruments are now available in near real time to the NWP community. Most NWP centres have undertaken major research and development efforts on the validation and assimilation of this new advanced infrared sounder.

The aim of the workshop is to review the critical issues related to the assimilation of high-spectral-resolution sounders in operational NWP centres, in particular monitoring, cloud detection, channel selection, data compression and radiative-transfer modelling.

The workshop attendance is by invitation only.

ECMWF 2004 Annual Seminar (6–10 September)

The one-week seminar in 2004 will be on "Developments in numerical methods for atmospheric and ocean modelling".

Objectives

The seminar will present a pedagogical review of recent developments in numerical methods for atmospheric and ocean modelling. Topics to be covered will include the choice of the basic dynamical equations and coordinate systems for different applications, and the virtues of various horizontal and vertical discretizations in the context of a range of resolutions. The choice of time-integration schemes and questions of accuracy and conservation will also be addressed. Issues of efficiency on different computer architectures will also be considered.

The balance between accuracy and discretization is an important issue in ocean wave modelling. As the power of computers becomes greater and greater, the resolution of even global models is reaching the point where non-hydrostatic effects have to be taken into account and efficient algorithms for avoiding instabilities in fast-travelling waves become of crucial importance.

Posters providing further information on the programme and application forms will be distributed around May 2004.

Seminar registration

Applications are open to all ECMWF Member States and Co-operating States. Other applicants should contact ECMWF for further information. A registration form will be made available around June 2004.

Contact address

Els Kooij-Connally
European Centre for Medium Range Weather Forecasts
Shinfield Park, Reading
Berkshire RG2 9AX
England
Tel.: UK 0118 949 9751; International +44 118 949 9751
Telex: 84708 ECMWF G
Fax: 0118 986 9450
Email: seminars@ecmwf.int

1st ECMWF workshop on High-Performance Networking (September)

ECMWF intends to hold the first workshop on high-performance networking in mid September. Exact dates and times and an agenda will be announced later.

The mailing list for invitations will include all subscribers to the high-performance networking forum Europe mailing list.

Objectives

The objectives of this workshop will be to bring together European users and vendors of high-performance networking technologies and to share thoughts on the technology deployments, trends and future directions.

The workshop will continue in the direction set by the high-performance networking forum Europe, whose last meeting was hosted by ECMWF on 11 October 2002.

11th Workshop on the Use of High-Performance Computing in Meteorology (25–29 October)

Objectives

Every second year the ECMWF hosts a workshop on the use of high-performance computing (HPC) in meteorology. In 2004 we will hold our 11th workshop in this well-established series. The emphasis of this workshop will be, as before, on achieving sustained teraflop performance in a production environment.

Our aim is to provide a venue where users from our Member States and around the world can report on their experience and achievements in the field of HPC during the last two years, and plans for the future and requirements for computing power will also be presented. Vendors of supercomputers will have the opportunity to talk to managers and end users of meteorological computer centres about their current and future products, and meteorological scientists can present their achievements in the development of parallel computing techniques and algorithms, and can exchange ideas on the use of supercomputers in future research. Computer scientists can give an update on their efforts in providing tools that will help users to exploit the power of supercomputers in the field of meteorology, and the challenges of creating a computer centre infrastructure for HPC can be discussed.

The workshop will consist of a limited number of presentations from invited speakers, plus a series of 20-minute contributions. The morning of the final day will be reserved for an open discussion session.

Attendance at the workshop is by invitation and will be limited to around 100 persons. If you are interested, please contact the workshop organizers:

By e-mail

hpcworkshop@ecmwf.int

By post

HPC Workshop
European Centre for Medium-Range Weather Forecasts
Shinfield Park
Reading/Berks.
RG2 9AX
United Kingdom

By telephone

UK 0118 949 9000; International +44 118 949 9000
Workshop administration: Hanna Mullane
Programme co-ordinator: George Mozdzynski

ECMWF/ELDAS workshop on land surface assimilation (8–11 November)

Details to be announced later.

ECMWF Calendar 2004

Meteorological Training Course

May 5-14 Data assimilation & use of satellite data
May 17-21 Predictability, diagnostics and seasonal forecasting

Jun 3-4 Council 60th
Jun 6-10 WISE meeting (Waves In Shallow-water Environment)

Meteorological Training Course

Jun 7-11 Use and interpretation of ECMWF products

Jun 14-16 Forecast products – Users Meeting
Jun 28-Jul 1 Workshop – Assimilation of high spectral resolution sounders in NWP
Sep 6-10 Seminar – Recent developments in numerical methods for atmosphere and ocean modelling

Oct 4-6 Scientific Advisory Committee 33rd
Oct 6-8 Technical Advisory Committee 34th

Meteorological Training Course for WMO Members

Oct 11-15 Use & interpretation of ECMWF products

Oct 12-13 Finance Committee 73rd
Oct 14-15 Policy Advisory Committee 21st
Oct Advisory Comm. of Co-operating States 11th
(to be decided)
Oct 25-29 Workshop – 11th workshop on High-Performance Computing in Meteorology
Nov 8-11 Workshop - ECMWF/ELDAS workshop on land-surface assimilation
Nov 29-30 Council 61st

New products on the ECMWF web site

Member State server

The new Member State server ecgate is an IBM p690 system with 16 Power4 processors. Full user service started on 21st January 2004. The current SGI server ecgate1 will remain in service in parallel until 31 July 2004. Details are on

http://www.ecmwf.int/services/computing/ecgate/

Computer Training Course

The Computer Training Course 2004 was held in February/March 2004. The course material is available on.

http://www.ecmwf.int/services/computing/training/material/

New building at ECMWF

Details of a new 'Invitation to Tender' for an extension to the ECMWF computer building are available on

http://www.ecmwf.int/newsevents/itt/

Earth-system monitoring

The objectives of the GEMS (Global Earth-system Monitoring using Satellite and in-situ data) project have been published on the Web and a draft version of a proposal for submission to the European Union's Sixth Framework Programme has been prepared. Further information is available on

http://wedit.ecmwf.int/research/EU_projects/GEMS/

Andy Brady

TAC Representatives, Computing Representatives and meteorological contact points

Member State	TAC Representative	Computer Representative	Meteorology Contact Point
Belgium	Dr D. Gallens	Mrs L. Frappez	Dr J. Nemeghaire
Denmark	Mr L. Laursen	Mr N. Olsen	Mr G. Larsen
Germany	Mr H.-J. Koppert	Ms E. Krenzien	Mr D. Meyer
Spain	Mr C. del Rio	Mr E. Monreal	Ms A. Casals Carro
France	Mr B. Strauss	Mrs M. Pithon	Mr J. Clochard
Greece	Mr J. Bassiakos	Major J. Alexiou	Mr I. Papageorgiou, Mr P. Xirakis
Ireland	Mr J. Logue	Mr P. Halton	Mr M. Walsh
Italy	T. Col. Dr S. Pasquini	Mr G. Tarantino	Dr G. Maresca
Luxembourg	Mr C. Alesch	Mr C. Alesch	Mr C. Alesch
Netherlands	Mr T. Moene	Mr H. de Vries	Mr J. Diepeveen
Norway	Mr J. Sunde	Ms R. Rudsar	Mr P. Evensen
Austria	Dr G. Wihl	Dr G. Wihl	Dr H. Gmoser
Portugal	Mrs I. Barros Ferreira	Mrs M. da C. Periera Santos Mr J. Monteiro	Mr F. Prates
Switzerland	Dr S. Sandmeier	Mr P. Roth	Mr R. Mühlebach
Finland	Mrs K. Soini	Mr K. Niemelä	Mr P. Nurmi
Sweden	Mr I. Karro	Mr R. Urrutia	Mr O. Åkesson
Turkey	Dr M. Demirtaş	Mr B. Yagci	Mr Ö. Yilmaz
United Kingdom	Dr A. Dickinson	Mr P. Dando	Mr A. Radford
Cooperating States			
Croatia	Dr B. Gelo	Mr V. Malović	Mr D. Glasnović
Czech Republic	Mr M. Janoušek	Mr M. Janoušek	
Hungary	Mr I. Mersich	Mr I. Ihász	Mr I. Ihász
Iceland	Mr K. G. Bjarnason	Mr K. G. Bjarnason	Mrs S. Karlsdottir
Romania	Dr D. Banciu	Mr C. Soci	Dr E. Cordoneanu, Dr O. Diaconu
Slovenia	Mr J. Jerman	Mr M. Razinger	Mr B. Gregorčič
Serbia/Montenegro	Ms L. Dekic	Mr V. Dimitrijević	

Member State	TAC Representative	Computer Representative	Meteorology Contact Point
Observers			
EUMETSAT	Mr M. Rattenborg	Dr K. Holmlund	
Finance Committee	Mrs C. de Sousa Monteiro		
Scientific Advisory Committee	Prof C. Schär		
WMO	Mr M. Jarraud		

ECMWF publications

(see http://www.ecmwf.int/publications/library/ecpublications/)

Technical Memoranda

410 **Tompkins, A.M.** and **M. Janisková**: A cloud scheme for data assimilation purposes: Description and initial tests. *June 2003*

413 **Prior, P.** (compiler): Report on the fifteenth meeting of computing representatives, 19-20 May 2003. *July 2003*

414 **Lalaurette, F., L. Ferranti, A. Ghelli, Ø. Saetra** and **H. Böttger**: Verification statistics and evaluations of ECMWF forecasts in 2001-2002. *July 2003*

415 **Massacand, A.**: Forecasting of extreme seasonal precipitation: Insight into the ECMWF potential. *September 2003*

416 **Ehrendorfer, M.** and **A. Beck**: Singular vector-based multivariate normal sampling in ensemble prediction. *August 2003*

417 **Vialard, J., F. Vitart, M.A. Balmaseda, T.N. Stockdale, D.L.T. Anderson**: An ensemble generation method for seasonal forecasting with an ocean-atmosphere coupled model. *July 2003*

418 **van Oldenborgh, G.J., M.A. Balmaseda, L. Ferranti, T.N. Stockdale, D.L.T. Anderson**: Did the ECMWF seasonal forecast model outperform a statistical model over the last 15 years? *September 2003*

419 **Keil, C.** & **A. Beljaars**: The impact of a new parametrization of turbulent orographic form drag. *August 2003*

420 **Prior, P.**: Report on the eleventh Security Representatives' meeting 15-16 May 2003. *September 2003*

421 **Seuffert, G., H. Wilker, P. Viterbo, M. Drusch** and **J-F. Mahfouf**: On the usage of screen-level parameters and microwave brightness temperature for soil moisture analysis. *October 2003*

422 **Jung, T., A. Tompkins**: Systematic errors in the ECMWF forecasting system. (SAC Paper) *October 2003*

424 **Vitart, F.**: Monthly forecasting system. (SAC Paper) *October 2003*

425 **Matricardi, M.**: RTIASI-4: A new version of the ECMWF fast radiative transfer model for the infrared atmospheric sounding interferometer. *October 2003*

426 **Coelho, C.A.S., S. Pezzulli, M. Balmaseda, F.J., Doblas-Reyes** and **D.B. Stephenson**: Skill of coupled model seasonal forecasts: A Bayesian assessment of ECMWF ENSO forecasts. *December 2003*

427 **Beljaars, A., A. Brown** & **N. Wood**: A new parametrization of turbulent orographic form drag. *November 2003*

428 **Dethof, A.**: Assimilation of ozone retrievals from the MIPAS instrument onboard ENVISAT. *December 2003*

430 **Nurmi, P.**: Recommendations on the verification of local weather forecasts. *December 2003*

431 **Tan, D.G.H.** and **E. Andersson**: Simulation of the yield and accuracy of wind profile measurements from the Atmospheric Dynamics Mission (ADM-Aeolus). *January 2004*

432 **Lalaurette, F., L. Ferranti, A. Ghelli** & **G. van der Grijn**: Verification statistics and evaluations of ECMWF forecasts in 2002-2003. *December 2003*

ERA-40 Reports

8 **A.K. Betts** and **A.C.M. Beljaars**: ECMWF ISLSCP-II near-surface dataset from ERA-40. *October 2003*

9 **Seneviratne, S.I., P. Viterbo, D. Lüthi** & **C. Schär**: Inferring changes in terrestrial water storage using ERA-40 reanalysis data: The Mississippi river basin. *November 2003*

10 **Jung, T., E. Klinker** and **S. Uppala**: Reanalysis and reforecast of three major European storms of the 20th century using the ECMWF forecasting system. *November 2003*

11 **F. Chevallier, A. Hernandez, G. Kelly, A. Simmons** and **S. Uppala** : High clouds over oceans in the ECMWF 15-year and 45-year re-analyses. *December 2003*

13 **Troccoli, A.** and **P. Kållberg**: Precipitation correction in the ERA-40 reanalysis. *February 2004*

ESA Reports

Dethof, A.: Monitoring of retrievals from the MIPAS and SCIAMACHY instruments onboard ENVISAT. Final report for ESA contract. *December 2003*

Seminar Proceedings

ECMWF Seminar Proceedings on Predictability of weather and climate. *9-13 September 2002*

ECMWF Seminar Proceedings on Recent Developments in Data Assimilation for Atmosphere and Ocean. *8-12 September 2003*

Workshop Proceedings

ECMWF Workshop on role of the upper ocean in medium and extended range forecasting 13-15 November 2002

ECMWF/SPARC Workshop on modelling and assimilation for the stratosphere and tropopause. 23-26 June 2003

EUMETSAT/ECMWF Fellowship Programme Research Report

RR14 **C. Köpken, J-N. Thépaut** and **G. Kelly**: Assimilation of geostationary WV radiances from GOES and Meteosat at ECMWF. *April 2003*

Miscellaneous reports

Verification of ECMWF products in Member States and Co-operating States – Report 2003

Index of past newsletter articles

This is a list of recent articles published in the ECMWF Newsletter series.
Articles are arranged in date order within each subject category. Articles can be accessed on the ECMWF public web site

http://www.ecmwf.int/pressroom/newsletter/ index.html

Useful names and telephone numbers within ECMWF

Telephone number of an individual at the Centre is:

International: +44 118 949 9 + three digit extension
UK: (0118) 949 9 + three digit extension
Internal: 2 + three digit extension

e.g. the Director's number is:
+44 118 949 9001 (international),
(0118) 949 9001 (UK) and 2001 (internal).

E-mail

The e-mail address of an individual at the Centre is:
firstinitial.lastname@ecmwf.int

e.g. the Director's address is: D.Burridge@ecmwf.int

Internet web site

ECMWF's public web site is: http://www.ecmwf.int

	Ext
Director	
David Burridge	001
Deputy Director and Head of Operations Department	
Dominique Marbouty	003
Head of Administration Department	
Gerd Schultes	007
Head of Research Department	
Philippe Bougeault	005
ECMWF switchboard	000
Advisory	
Internet mail addressed to Advisory@ecmwf.int	
Telefax (+44 118 986 9450, marked User Support)	
Computer Division	
Division Head	
Walter Zwieflhofer	050
Computer Operations Section Head	
Sylvia Baylis	301
Networking and Computer Security Section Head	
Matteo Dell'Acqua	356
Servers and Desktops Section Head	
Richard Fisker	355
Systems Software Section Head	
Neil Storer	353
User Support Section Head	
Umberto Modigliani	382
User Support Staff	
John Greenaway	385
Norbert Kreitz	381
Dominique Lucas	386
Carsten Maaß	389
Pam Prior	384
Computer Operations	
Call Desk	303
Call Desk email: cdk@ecmwf.int	
Console - Shift Leaders	803
Console fax number +44 118 949 9840	
Console email: newops@ecmwf.int	
Fault reporting - Call Desk	303
Registration - Call Desk	303
Service queries - Call Desk	303
Tape Requests - Tape Librarian	315
Software libraries (eclib, nag, etc.)	
John Greenaway	385

	Ext
ECMWF library & documentation distribution	
Els Kooij-Connally	751
Meteorological Division	
Division Head	
Horst Böttger	060
Applications Section Head	
Alfred Hofstadler	400
Data and Services Head	
Baudouin Raoult	404
Graphics Section Head	
Jens Daabeck	375
Operations Section Head	
François Lalaurette	420
Meteorological Analysts	
Antonio Garcia Mendez	424
Federico Grazzini	421
Anna Ghelli	425
Meteorological Operations Room	426
Data Division	
Division Head	
Adrian Simmons	700
Data Assimilation Section Head	
Erik Andersson	627
Satellite Section Head	
Jean-Nöel Thépaut	621
Reanalysis Project (ERA)	
Saki Uppala	366
Probability Forecasting & Diagnostics Division	
Division Head	
Tim Palmer	600
Seasonal Forecasting Head	
David Anderson	706
Model Division	
Division Head	
Martin Miller	070
Numerical Aspects Section Head	
Mariano Hortal	147
Physical Aspects Section Head	
Anton Beljaars	035
Ocean Waves Section Head	
Peter Janssen	116
Education & Training	
Renate Hagedorn	257
GMES Coordinator	
Anthony Hollingsworth	824